DAMPING AND SATURATION OF A SECOND ORDER ELECTRON PLASMA WAVE ECHO

Thesis by

Charles P. Moeller

In partial fulfillment of the requirements

for the degree of

Doctor of Philosophy

California Institute of Technology

Pasadena, California

1973

(Submitted January 10, 1973)

ACKNOWLEDGMENT

The author wishes to express his gratitude for the help received in preparing this thesis. Professor Roy W. Gould suggested the problem and provided encouragement and many useful suggestions throughout the course of the work. Dr. Robert S. Harp also supervised the work in Professor Gould's absence. The author is very grateful to Keith Burrell, Richard Smith and John Wilgen for encouragement and many useful suggestions. Many thanks are due Mrs. Ruth Stratton for her patience and skill in typing the manuscript. The author gratefully acknowledges the financial assistance he received from Caltech and the support of this research by the A.E.C.

ABSTRACT

A description is given of experimental work on the damping of a second order electron plasma wave echo due to velocity space diffusion in a low temperature magnetoplasma. Sufficient precision was obtained to verify the theoretically predicted cubic rather than quadratic or quartic dependence of the damping on exciter separation. Compared to the damping predicted for Coulomb collisions in a thermal plasma in an infinite magnetic field, the magnitude of the damping was approximately as predicted, while the velocity dependence of the damping was weaker than predicted. The discrepancy is consistent with the actual non-Maxwellian electron distribution of the plasma.

In conjunction with the damping work, echo amplitude saturation was measured as a function of the velocity of the electrons contributing to the echo. Good agreement was obtained with the predicted J_1 Bessel function amplitude dependence, as well as a demonstration that saturation did not influence the damping results.

TABLE OF CONTENTS

INTRODUCTION

A plasma can support longitudinal oscillations of its charged particles which involve purely electrostatic interactions. Landau [1] first correctly determined the dispersion relation for the associated initial value problem for a plasma with a non-zero electron temperature.

A most important result of Landau's analysis is a damping of these oscillations even in the complete absence of collisions. The damping arises because the oscillations are not those of some normal mode of the plasma, but rather, as van Kampen [2] showed, the macroscopic manifestation of an infinity of normal modes which, because of the thermal spread in velocities, get out of phase. The oscillations that appear are determined by which modes are excited and by how particle interactions reinforce certain modes. The greater the spread in velocities involved, the more rapid the damping will be, because the macroscopic quantities involve integrals over velocity.

The boundary value problem concerning these oscillations was also examined by Landau [1]. In this case, electrons perturbed by an oscillating charge sheet produce an oscillating electric field as their thermal energy carries them away from the exciter. Because of the thermal spread in velocities, the electrons which were initially contributing in phase to the electric field get out of phase, resulting in a damping of the macroscopic electric field with distance from the exciter.

At frequencies comparable to the electron plasma frequency the ions cannot follow the electron motion and can be considered stationary. However, for sufficiently low frequencies, the ions can follow the

electron motion to produce another branch of the electrostatic wave dispersion relation which also contains collisionless damping. Gould [3] computed the dispersion relation for the steady state ion waves, and observed that unlike Landau's initial value problem, the analysis of which finally resulted in integration over a single dominant pole, the steady state problem had no single dominant pole, so that a numerical solution of the dispersion relation was required.

All of the experimental verification of Landau damping has been for the steady state problem, because the short time intervals involved in the initial value problem are experimentally difficult. Landau damping of the electron branch has been observed by Wong et al [4], Malmberg and Wharton [5], and Malmberg et al [6]. Landau damping of the ion branch has been observed by Wang [10].

The experimental verification of the dispersion relation for longitudinal waves does not, however, give direct demonstration of the most interesting feature of the damping. That is, in the absence of collisions, the distribution function of the electrons or ions does not relax to a time independent function, but retains the information necessary to determine the distribution at any previous time or position.

A method by which the phase mixing could be reversed was proposed by Gould, O'Neil, and Malmberg [7,8,9], based on a perturbation expansion in applied fields of the Vlasov equation. In the steady state case, this reversal is accomplished by locating two axially separated exciters of different frequencies in the plasma, as shown in the following figure.

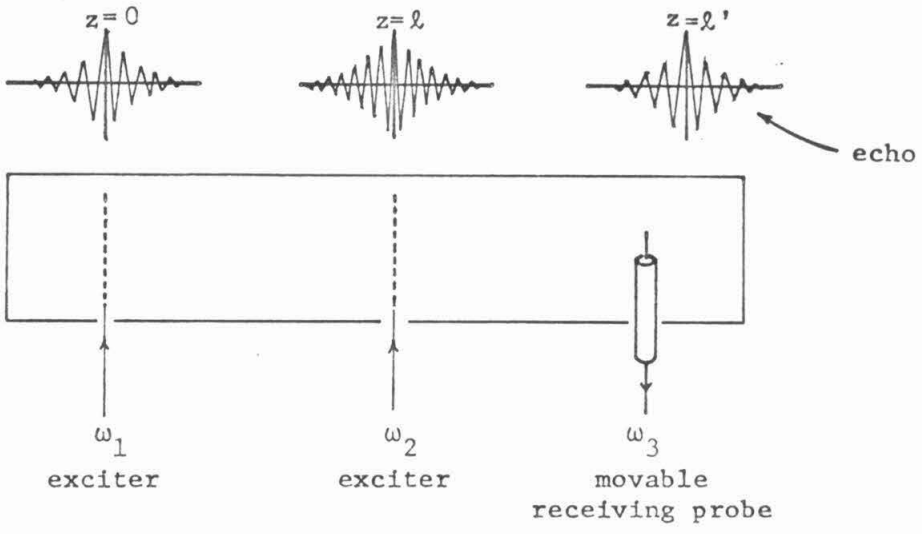

Electrons from $z < 0$ moving to the right due to their thermal energy pass through the first exciter and receive a small change in velocity. This modulation of the distribution function produces a charge imbalance of frequency ω_1 which is propagated away from the exciter by the thermal motion of the electrons. The thermal spread in the velocities of the electrons causes the electric field of this density wave to damp with increasing distance from the exciter due to phase mixing even though, in the absence of collisions, the perturbation in the distribution function remains.

The electrons which were perturbed by the first exciter continue to travel past the second exciter where they experience a perturbation at frequency ω_2. The electric field of the wave launched by the second exciter of frequency ω_2 also phase mixes away. The ω_2 perturbation also initiates a reversal of the phase mixing which the ω_1

perturbation has undergone, so that as the electrons continue to travel to the right, at a certain position they come back into phase, producing a response of frequency $\omega_3 = \omega_2 - \omega_1$ at $z = \ell' = \ell\omega_2/\omega_3$. This is shown in Chapter I.

The spatial plasma wave echo was first experimentally observed by Malmberg, Wharton, and Gould [12]. The spatial ion wave echo was observed by Ikezi, Takahashi and Nishikawa [13] and Baker et al [14].

The perturbed distribution which produces the echo will be altered, however, by collisions. Large angle collisions such as electron-neutral collisions will completely destroy the memory which the electrons have of previous perturbations, so that one would expect a simple exponential damping of the echo with exciter separation. Small angle Coulomb collisions, however, have a more subtle effect, only altering the electron velocity slightly, but with a randomness which leads to an additional phase mixing which cannot be undone. As was shown by Karpman[15], Su and Oberman [16], and Dupree [17], the Coulomb collisions or turbulence cause the perturbed distribution function to damp exponentially as the third power of the distance from the exciter.

Using the damping of the perturbed distribution, O'Neil [18] and Su and Oberman [16] gave the damping due to diffusion in velocity space for electron plasma wave echoes while Nishikawa and Gould [19] computed the damping of ion wave echoes. Hinton [20] considered the damping of an electron beam echo by velocity space diffusion.

An experimental study of the damping of second order ion wave echoes which agrees well with the theory was done by Wong and Baker [21] on a Q machine. The second order ion wave echo has the disadvantage,

however, that particles with a large range of velocities contribute to the echo, so that it is difficult to get a measure of the velocity dependence of the damping.

Guillemot et al [22] and Jensen et al [23] avoid this difficulty to a large degree by using a resonant third order electron plasma wave echo. With the resonant echo, the transmitting and receiving frequencies are all the same, so that the only velocities involved are in a narrow range around ω/k, where ω is the echo frequency and k is the corresponding wave number. The results reported on the dependence of damping with distance are consistent with the theory, but there is not enough precision to prove the dependence. Further, they have not given any indication of velocity dependence. The theoretical velocity dependence of the damping is very strong, so even a narrow range of velocities in the echo could give an incorrect distance dependence. These works were also distinguished by the use of a broadband noise source to produce a known turbulence.

This work describes a measurement of the spatial and velocity dependence of the electron plasma wave echo damping due to Coulomb collisions and also a measurement of the amplitude saturation of the echo. This work is distinguished by the use of a relationship in the echo between the velocity of electrons producing the echo and the spatial Fourier components of the echo electric field. By moving a receiving probe through the region containing the echo electric field and using a detector sensitive to phase (with reference to the applied signals) as well as amplitude, one can obtain from a record of the

detected signal as a function of probe position information about the phenomena of interest for all electron velocities represented in the perturbed distribution of the echo.

This information is obtained by taking the spatial Fourier transform of the recorded echo amplitude, a Fourier component from which represents the contribution to the echo of electrons of a corresponding velocity.

In particular, by examining echoes produced with various spacings between exciters, one can observe for a given Fourier component from each echo, the effect of collisions on the electrons of the corresponding velocity. Because the predicted damping has a very strong velocity dependence, this technique was also necessary just to determine the dependence of damping on distance.

The theory of damping referred to above uses a perturbation expansion of the distribution function in the applied amplitudes. This theory gives an echo amplitude which is proportional to the two applied amplitudes and also to the exciter separation ℓ . Experimentally, as the amplitude or exciter separation is increased, the echo amplitude increases more slowly, reaches a maximum, and then decreases, and is said to saturate. An analysis based on the perturbed ballistic motion of the electrons rather than the Vlasov equation (in the absence of collisions) by Gould [8,9] and in more detail by Coste and Peyraud [11], gives the echo for arbitrary amplitudes and demonstrates the nonsymmetric roles of the two exciters.

By keeping the exciter separation fixed and examining echoes produced with various applied amplitudes, from a given Fourier component the amplitude behavior of the contribution to the echo of electrons of the corresponding velocity was obtained. From this data the effect of saturation on the damping measurements was determined to be negligible.

In Chapter I the quantitative behavior of the echo is derived. The echo damping, echo saturation effects, and the velocity diffusion coefficient in a magnetic field are obtained.

In Chapter II the plasma and its diagnostics and the experimental apparatus and procedures are described.

In Chapter III the experimental results and their comparison with theory are given.

I. THEORY OF THE ECHO

1.1 Reduction to a One-Dimensional Problem

All the phenomena of interest in this work are governed by the Boltzmann equation for the electrons with a Focker-Planck collision term,

$$\frac{\partial F}{\partial t} + \vec{v} \cdot \nabla_r F + \frac{e}{m}(\vec{E} + \vec{v} \times \vec{B}) \cdot \nabla_v F = \frac{\partial}{\partial v_i}(FD_i) + \frac{\partial^2}{\partial v_i \partial v_j}(FD_{ij}) \qquad (1)$$

It is assumed that there is a static magnetic field B_o in the z direction and no static electric field. D_i and D_{ij} are the coefficients of dynamical friction and diffusion, which will be discussed in Section 5. The ions are assumed stationary.

Separating static quantities from time dependent quantities in (1) by writing $F(\vec{r},\vec{v},t) = F_o(r_x,r_y,\vec{v}) + F_1(\vec{r},\vec{v},t)$, $\vec{E}(\vec{r},t) = \vec{E}_1(\vec{r},t)$, and $\vec{B}(\vec{r},t) = \vec{B}_o + \vec{B}_1(\vec{r},t)$, one obtains

$$\vec{v} \cdot \nabla_r F_o + \frac{e}{m}\vec{v} \times \vec{B}_o \cdot \nabla_r F_o = \frac{\partial}{\partial v_i}(F_o D_i) + \frac{\partial^2}{\partial v_i \partial v_j}(F_o D_{ij}) \qquad (2a)$$

and

$$\frac{\partial F_1}{\partial t} + \vec{v} \cdot \nabla_r F_1 + \frac{e}{m}\vec{v} \times \vec{B}_o \cdot \nabla_v F_1 = -\frac{e}{m}\vec{E}_1 \cdot \nabla_v (F_o + F_1) - \frac{e}{m}\vec{v} \times \vec{B}_1 \cdot \nabla_v F_1$$

$$+ \frac{\partial}{\partial v_i}(D_i \cdot F_1) + \frac{\partial^2}{\partial v_i \partial v_j}(D_{ij} F_1) \qquad (2b)$$

We first wish to show that for sufficiently strong $\vec{B}_o$, this equation reduces to a one-dimensional equation in the z coordinate. In order to do this, we obtain a formal solution for F_1 by evaluating F_1 along an unperturbed trajectory given by $\vec{r}(\vec{r}_o,\vec{v}_o,t|t_o)$,

$\vec{v}(\vec{r}_o,\vec{v}_o,t|t_o)$, where $\vec{r}$ and $\vec{v}$ equal $\vec{r}_o$ and $\vec{v}_o$ for $t = t_o$.

Let

$$g(\vec{r},\vec{v},t) = -e/m\ \vec{E}_1\cdot\nabla_v(F_o+F_1) - \frac{e}{m}\vec{v}\times\vec{B}_1\cdot\nabla_v F_1 + \frac{\partial}{\partial v_i}(F_1 D_i) + \frac{\partial^2}{\partial v_i \partial v_j}(F_1 D_{ij}) \qquad (3)$$

Integrating along the trajectory, one obtains

$$F_1(\vec{r}(\vec{r}_o,\vec{v}_o,t|t_o),\ \vec{v}(\vec{r}_o,\vec{v}_o,t|t_o),t) = \int_{t_o}^{t} g(\vec{r}(\vec{r}_o,\vec{v}_o,t'|t_o),\ \vec{v}(\vec{r}_o,\vec{v}_o,t'|t_o),t')dt'$$

and then, using the Jacobian $\dfrac{\partial[\vec{r}(\vec{r}_o,\vec{v}_o,t|t_o),\ \vec{v}(\vec{r}_o,\vec{v}_o,t|t_o)]}{\partial[\vec{r}_o,\vec{v}_o]} = 1$,

$$F_1(\vec{r},\vec{v},t) = \int\int\int_{t_o}^{t} g(\vec{r}(\vec{r}_o,\vec{v}_o,t'|t_o),\ \vec{v}(\vec{r}_o,\vec{v}_o,t'|t_o),t')\ \delta(\vec{r}-\vec{r}(\vec{r}_o,\vec{v}_o,t|t_o))\delta(\vec{v}-\vec{v}(\vec{r}_o,\vec{v}_o,t|t_o))dt'd^3r_o d^3v_o \qquad (4a)$$

If one chooses the time t' instead of t_o to define the initial conditions, one can change variables in (4a) to give

$$F_1(\vec{r},\vec{v},t) = \int\int\int_{0}^{t-t_o} g(\vec{r}_o',\vec{v}_o',t-t'')\ \delta(\vec{r}-\vec{r}(\vec{r}_o',\vec{v}_o',t|t-t''))\times\ \delta(\vec{v}-\vec{v}(\vec{r}_o',\vec{v}_o',t|t-t''))dt''d^3r_o'd^3v_o' \qquad (4b)$$

Using the matrix $M = \begin{pmatrix} 0 & 1 \\ -1 & 0 \end{pmatrix}$ and $I = \begin{pmatrix} 1 & 0 \\ 0 & 1 \end{pmatrix}$, the unperturbed motion is given by

$$z(\vec{r}_o,\vec{v}_o,t|t_o) = z_o + v_{oz}(t-t_o) \tag{5a}$$

$$v_z(\vec{r}_o,\vec{v}_o,t|t_o) = v_{oz} \tag{5b}$$

$$\vec{r}_\perp(\vec{r}_o,\vec{v}_o,t|t_o) = \vec{v}_{o\perp} - \frac{M}{\omega_c}\cdot(\exp[M\omega_c(t-t_o)] - I)\cdot\vec{v}_{o\perp} \tag{5c}$$

$$\vec{v}_\perp(\vec{r}_o,\vec{v}_o,t|t_o) = \exp[M\omega_c(t-t_o)]\cdot\vec{v}_{o\perp} \tag{5d}$$

where $\omega_c = eB_o/m$, and the "$\perp$" means in the plane perpendicular to $\vec{B}_o$. Integration over the δ functions gives

$$F_1(\vec{r},\vec{v},t) = \int_0^{t-t_o} g[\vec{r}_\perp + \frac{M}{\omega_c}\cdot(\exp[-M\omega_c t'] - I)\cdot\vec{v}_\perp, z-v_z t', \times \exp[-M\omega_c t']\cdot\vec{v}, v_z, t-t']dt' \tag{6}$$

The expression following $\vec{r}_\perp$ in the argument of g in (6) clearly $\to 0$ as $\omega_c \to \infty$.

By integrating $F_1(\vec{r},\vec{v},t)$ over $\vec{v}_\perp$, one can define new distribution functions $f_1(\vec{r},\vec{v}_z,t) = \int\int_{-\infty}^{\infty} F_1(\vec{r},\vec{v},t)\, dv_x dv_z$ and $f_o = \int\int_{-\infty}^{\infty} F_o\, dv_x dv_z$.

$$f_1(\vec{r},v,t) = \int_0^{t-t_o}\int\int_{-\infty}^{\infty} g[\vec{r}_\perp, z-v_z t', \exp[-M\omega_c t']\,\vec{v}_\perp, v_z, t-t']d^2v_\perp dt'$$

For a given t', one can make a change of variable in the $\vec{v}_\perp$ integral, a rotation of $\vec{v}_\perp$, to obtain

$$f_1(\vec{r},v,t) = \int_0^{t-t_o}\int\int_{-\infty}^{\infty} g(\vec{r}, z-vt', \vec{v}_\perp', v, t-t')\, d^2v_\perp' dt' \quad .$$

Using the definition (3) of g, integration by parts, the fact that F_o and $F_1 \to 0$ as $\vec{v} \to \infty$, and assuming that F_o and F_1 are even functions of v_x and v_y, one obtains

$$f_1(\vec{r},v,t) = \int_0^{t-t_o} -\frac{e}{m} E_1(\vec{r},t-t') \frac{\partial}{\partial v}(f_o + f_1) + \frac{\partial}{\partial v} \int\int_{-\infty} F_1 D_3 d^2v + \frac{\partial^2}{\partial v^2} \int\int_{-\infty}^{\infty} F_1 D_{33} d^2v_\perp' \quad dt' \tag{7}$$

If one assumes F_1/f_1 is a function only of v, one can write

$$\int\int_{-\infty}^{\infty} F_1 D_3 d^2v = f_1 \tilde{D}_3 \quad \text{and} \quad \int\int_{-\infty}^{\infty} F_1 D_{33} d^2v = f_1 \tilde{D}_{33}$$

Equation (7) is then equivalent to

$$\frac{\partial f_1}{\partial t} + v \frac{\partial f_1}{\partial z} + \frac{e}{m} E_{1z} \frac{\partial (f_o + f_1)}{\partial v} = \frac{\partial}{\partial v} (f_1 \tilde{D}_3) + \frac{\partial^2}{\partial v^2} (f_1 \tilde{D}_{33}) \tag{8}$$

f_o and f_1 do not have a $\perp$ velocity dependence, but they still depend on $r_\perp$.

If one takes only first order terms in the perturbed quantities and initially ignores damping (which only becomes important for large distances), by doing a spatial and temporal Fourier transform of (8) one obtains

$$\hat{f}_1(\vec{r}_\perp,k,\omega,v) = i \frac{e}{m} \frac{E_{1z}(\omega,k,\vec{r}_\perp)}{\omega - kv} \frac{\partial f_o}{\partial v} (\vec{r}_\perp,v)$$

Defining $\rho_p = e \int_{-\infty}^{\infty} \hat{f}_1 dv$ and $\rho_e = \varepsilon_o \nabla \cdot \vec{E}_e$, where $\vec{E}_e$ is the external

perturbing field, one can use $\varepsilon_o \nabla \cdot \vec{E}_1 = \rho_e + \rho_p$ to obtain

$$\varepsilon_o \nabla \cdot \vec{E}_1 - \rho_e = \frac{1}{k} \frac{e^2}{m\varepsilon_o} \int_{-\infty}^{\infty} \frac{(\partial f_o(\vec{r}_\perp, v))/\partial v}{\omega - kv} dv \; ik\varepsilon_o E_{1z}$$

Letting $\vec{E} = -\nabla\phi$ and defining $\varepsilon(\omega,k,\vec{r}_\perp) = 1 - \frac{e^2}{k^2 m\varepsilon_o} \times \int_{-\infty}^{\infty} \frac{\partial f_o/\partial v}{\omega - kv} dv$,

$$-\varepsilon_o \left(\frac{\partial^2\phi}{\partial x^2} + \frac{\partial^2\phi}{\partial y^2} - k^2\phi\right) - \rho_e = (1 - \varepsilon(\omega,k,\vec{r}_\perp))k^2\varepsilon_o\phi \qquad (9)$$

$\frac{\partial^2\phi}{\partial x^2} + \frac{\partial^2\phi}{\partial y^2} - k^2\varepsilon(\omega,k,\vec{r}_\perp)\phi = -\rho_e/\varepsilon_o$. If the excitation ρ_e is independent of azimuthal angle and the plasma is assumed to be a cylindrical column, the boundary conditions are $\partial\phi/\partial r = 0$ at $r = 0$ and $\phi = 0$ at r=a, where a is the radial boundary and $r = |r_\perp|$.

For a Maxwellian plasma, $\varepsilon(\omega,k,r_\perp)$ can be expressed as $1 - \frac{\omega_p^2(r)}{\omega^2} \zeta^2 Z'(\zeta)$, where $\zeta = \omega/kv_{th}$, v_{th} is the thermal speed, ω_p is the plasma frequency, and $Z(\zeta)$ is the plasma dispersion function (Fried and Conte [31]). $|\zeta^2 Z'(\zeta)| \leq 1.6$, so that for ω sufficiently large, ε is weakly dependent on r . In this experiment $(\omega_p/\omega)^2 \leq \frac{1}{6}$. Then for k large compared to $1/a$ and r small compared to a , $\phi(r) \tilde{=} \rho_e/(\varepsilon_o\varepsilon(\omega,k,0))$, which is the solution of (9) for an infinite uniform plasma.

The same dielectric function arises in higher order phenomena, so that the same considerations apply. Therefore, all the subsequent analyses will be for the infinite plasma case. Henceforth, $\varepsilon(\omega,k)$ is defined as $\varepsilon(\omega,k,0)$.

1.2 The First Order Solution

Following the procedure of O'Neil, by assuming that collisional effects are only important many Landau damping lengths from the excitation, one can first solve the collisionless problem and then use that solution as an initial condition for the collisional problem.

Spatially and temporally Fourier transforming (8) and neglecting damping, one obtains

$$\hat{f}_1(k,v,\omega) = (\rho_e + \rho_p) \frac{e}{m\varepsilon_o k} \frac{(\partial f_e/\partial v)}{kv - \omega}$$

which gives

$$\hat{f}_1 = \frac{\rho_e(\omega,k)}{\varepsilon(\omega,k)} \frac{e}{m\varepsilon_o k} \frac{(\partial f_e/\partial v)}{kv - \omega} \tag{10}$$

where ρ_e and ρ_p have the same meaning as in Section 1.1.

With the time dependence taken as $\exp[-i\omega t]$, ω is given a small positive imaginary part. If dipole charge sheets at $z = 0$ are used for excitation, $\rho_e(\omega,k)/k$ remains finite as $k \to 0$. If ω is large compared to ω_p, $\varepsilon(\omega,k)$ has no zeroes near the real axis.

The inverse transform of (10) is

$$f_1(z,v,\omega) = \frac{1}{2\pi} \frac{e}{m\varepsilon_o} \frac{2f_o}{\partial v} \frac{1}{v} \int_{-\infty}^{\infty} \frac{\rho_e(\omega,k)}{k} \frac{1}{\varepsilon(\omega,k)} \frac{e^{ikz}}{k - \frac{\omega + i\delta}{v}} dk \tag{11}$$

For large z, only the $k = \omega/v$ term will contribute significantly to the integral in (11). For $z > 0$, one can close the contour in the positive imaginary plane, giving

$$f_1(z,v,\omega) = i\,\frac{e}{m\varepsilon_o}\,\frac{\partial f_o}{\partial v}\,\frac{1}{v}\,\frac{\rho_e(\omega,\omega/v)}{\omega/v}\,\frac{e^{i\omega z/v}}{\varepsilon(\omega,\omega/v)} \tag{12}$$

while for $v < 0$, $f_1(\omega,z,v) = 0$. The $f_1=0$ arises because electrons at $z > 0$ traveling in the -z direction cannot have been perturbed by an excitation at $z = 0$.

If ε is taken as 1, it is possible to estimate the decay of the perturbed density ρ_p (and therefore of ϕ and E_1). With $\rho_e(\omega,k)$ for a dipole charge sheet, $\rho_e = -ikD$, where D is the dipole moment, and integration of (12) over v gives

$$\rho_p(z) = \frac{e^2}{m\varepsilon_o} D \int_0^\infty \frac{1}{v}\frac{\partial f_o}{\partial v} e^{i\omega z/v}\, dv$$

$$= \frac{-e^2 D}{m\varepsilon_o \sqrt{\pi}\, v_{th}^2} \int_0^\infty \exp[-u^2 + ia/u]\, du$$

where $a = \omega z/(\sqrt{2}\, v_{th})$.

Using the saddle point approximation,

$$\rho_p(z) \overset{\sim}{=} \frac{-e^2 D}{m\varepsilon_o \sqrt{\pi}\, v_{th}^2} (\pi/3)^{1/2} \exp(3/4)(-1 + i\sqrt{3})a^{2/3}/2^{1/3}]$$

Using the experimental electron temperature and a frequency of 250 MHz, $|\rho_p(z)|$ varies as $\exp[-3.1z^{2/3}]$, z in cm. This damping length is short compared to the damping length for Coulomb collisions.

Therefore, for a sufficient distance from the exciter, $f_1(z,v,\omega) = F(\omega,v) \exp(i\omega z/v)$, F defined by (12). This satisfies

$$i\omega f_1 + v\frac{\partial f_1}{\partial z} = \frac{\partial(f_1\tilde{D}_3)}{\partial v} + \frac{\partial^2(f_1\tilde{D}_{33})}{\partial v^2} \quad . \tag{13}$$

when the collisions are negligible. The second collision term of (13) dominates the first, for at large z ,

$$\frac{\partial^2}{\partial v^2}(\tilde{D}_{33}f_1) \simeq \frac{-\omega^2 z^2}{v^4}\tilde{D}_{33} \quad , \text{ while}$$

$$\frac{\partial}{\partial v}(\tilde{D}_3 f_1) \simeq \frac{i\omega z}{v^2}\tilde{D}_3 \quad .$$

$\tilde{D}_{33}/\tilde{D}_3$ is usually of the order of v_{th}^2/v. In this experiment, the v of interest is $\sim 2v_{th} \simeq 10^8$ cm/sec, while $\omega \simeq 2\times 10^9$ and $z \simeq 10$ cm. This implies the ratio of the diffusion to dynamical friction term is $\omega z/2v$ or about 50 . With the velocity dependence of $\tilde{D}_{33}$ varying between 1 and $1/v^3$ (as will be shown later), its derivatives can also be ignored compared to $\exp[i\omega z/v]$.

$\partial F(\omega,v')/\partial v$ will also be assumed to be small compared to $\exp(i\omega z/v)$.

To solve the collisional equation (13), one may try a solution of the form

$$f_1 = e^{g(z,v)}\, e^{i\omega z/v}\, F(v,\omega) \quad .$$

One then has $-i\omega f_1 + v[\partial g/\partial z + i\omega/v]f_1 = -\omega^2 z^2 f_1 D_{33}/v^4$, where $\partial g/\partial v$ has also been ignored. This gives

$$\frac{\partial g}{\partial z}(z,v) = -\omega^2 z^2\, \tilde{D}_{33}/3v^5$$

which is satisfied by

$$g(z,v) = - \omega^2 z^3 \tilde{D}_{33}/3v^5 + h(v) \quad .$$

In order that the damping be small for short distances, $h(v)$ must be zero. In these experiments $|g| \leq 5$ so that $\left|\frac{\partial g}{\partial v}\right| < 5/v$, which is still small compared to $\left|\frac{\partial}{\partial v} \exp(i\omega z/v)\right| \simeq 10^2/v$. The result $\exp[-\omega^2 z^3 \tilde{D}_{33}/3v^5]$ for the damping was obtained by Karpman [15] and Su and Oberman [16].

In order to use this perturbed distribution in a nonlinear equation, one should either use only its real part or, what is equivalent, Fourier transform the equation in time and use both positive and negative frequencies.

Because the nonlinearity in the Boltzmann equation comes from the product of two such quantities, one can most easily obtain the correct result by using the complex conjugate of one factor, and then take half the real part of the final result.

1.3 The Second Order Echo

If the electrons with perturbed distribution

$$f_1^*(z,v,\omega_1) = F^*(\omega_1,v)\ \exp[-i\omega_1 z/v = \omega^2 z^3\ \tilde{D}_{33}(3v^5] \tag{14}$$

are perturbed again at $z = \ell$ by an electric field $E(z,\omega_2)$, a second order effect in exciting amplitude produces a distribution $f_2(z,v,\omega_3)$ with $\omega_3 = \omega_2 - \omega_1$ which satisfies

$$-i\omega_3 f_2 + v\,\frac{\partial f_2}{\partial v} + \frac{e}{m}\,E(z,\omega_3)\,\frac{\partial f_o}{\partial v} + \frac{e}{m}\,E(z,\omega_2)\,\frac{f_1^*(z,v,\omega_1)}{\partial v}$$

$$= \frac{\partial^2}{\partial v^2}\,(\tilde{D}_{33} f_2) \tag{15}$$

where

$$\varepsilon_o\,\frac{\partial E(z,\omega_3)}{\partial z} = e\int_{-\infty}^{\infty} f_2(z,v,\omega_3)\ dv$$

By ignoring the collisional term in (15) for small ℓ, one has left a first order linear equation with solution

$$f_2 = -\exp[i\omega_3 z/v]\,\frac{e}{m}\,\frac{1}{v}\,\frac{\partial f_o}{\partial v}\int_{z_o}^{z}\exp[-i\omega_3 z'/v]\,E(z',\omega_3)dz'$$

$$-\exp[i\omega_3 z/v]\,\frac{e}{mv}\int_{z_o}^{z}E(z',\omega_2)\,\frac{\partial f_1^*}{\partial v}(z',v,\omega_1)$$

$$\times\ \exp[i\omega_3 z'/v]\,dz' \quad , \qquad z_o << \ell \ . \tag{16}$$

The $E(z,\omega_3)$ in (16) is the electric field due to f_2, which can be consistently taken to be zero for small $z-\ell$. If one further assumes that $E(z,\omega_2)$ is localized around $z=\ell$, one can evaluate the damping at $z=\ell$.

$$f_2 \overset{\sim}{=} \frac{-i\omega_1}{v^3}\,\frac{e}{m}\exp[i\omega_3 z/v - D_{33}\omega_1^2\ell^3/3v^5 - i\omega_3\ell/v$$

$$- i\omega_1\ell/v]F^*(\omega_1,v)\int_{z_o}^{z}E(z',\omega_2)\exp[-i\omega_2(z'-\ell)/v]dz' \tag{17}$$

For z such that the field $E(z,\omega_2)$ has damped away, the integral in (17) is just the Fourier transform $\hat{E}(\omega_2/v,\omega_2)$. It is obtained by integrating (10) over v to give $\rho_p(\omega,k) = \rho_e(\omega,k)$ $\times(1-\varepsilon(\omega,k))/\varepsilon(\omega,k)$, which in turn yields $\hat{E}(k,\omega_2) = -i\rho_e/[k\varepsilon_o\varepsilon(\omega,k)]$, where ρ_e comes from the exciting electric field.

The exponential part of (17) is a rapidly oscillating function of v and therefore f_2 produces no electric field except for z near $\ell' = \omega_2\ell/\omega_3$.

In the region in between ℓ and ℓ', f_2 evolves according to (15), with the electric fields both zero, to give

$$f_s = \frac{-i\omega_1 \ell}{v^3} \frac{e}{m} \hat{E}(\omega_2/v, \omega_2)\ F^*(\omega_1, v)$$

$$\times\ \exp[i\omega_3 z/v - i\omega_2 \ell/v - \omega_1^2 \ell^3 \tilde{D}_{33}/3v^5 - \omega_3^2 (z-\ell)^3\ \tilde{D}_{33}/3v^5] \qquad (18)$$

Near ℓ', the electric field produced by f_2 modifies the distribution function, as indicated in (15). By evaluating the damping term at $z = \ell'$, it is possible to get a simple explicit expression for f_2 and its associated electric field. This approximation was also made by O'Neil [18] and Su and Oberman [16].

Let the solution of (15) with self-consistent fields included be given by $f_2 = f_S + f_R$, with $f_S = G(v,\ell) \exp[i\omega_3 (z-\ell')/v]$ where G is defined by (18). Then (15) reduces to

$$-i\omega_3 f_R + v \frac{\partial f_R}{\partial z} + \frac{e}{m} E(z, \omega_3) \frac{\partial f_o}{\partial v} = 0$$

$$\frac{\partial}{\partial z} E(\omega_3, z) = e \int_{-\infty}^{\infty} (f_S + f_R)\ dv \equiv \rho_S + \rho_R$$

Doing a spatial Fourier transform around $z = \ell'$, one obtains

$$\hat{f}_R(\omega_3, k) = -i \frac{e}{m} \frac{\hat{E}(k, \omega_3)\ \partial f_o/\partial v}{\omega - kv} \qquad (19)$$

and

$$ik\varepsilon_o \hat{E}(\omega_3, k) = e \int_{-\infty}^{\infty} \hat{f}_R\ dv + \frac{2\pi e \omega_3}{k^2} G(\omega_3/k, \ell) \quad .$$

Integrating over v in (19), one has

$$ik\,\varepsilon_o E(\omega_3,k) = \frac{2\pi e\omega_3}{k^2}\, G(\omega_3/k,\ell) \,/\, \varepsilon(\omega_3,k)$$

or

$$E(\omega_3,k) = \frac{2\pi\, e}{k^2 \varepsilon(k,\omega_3)\ \varepsilon_o}\ \frac{e}{m}\ E^*(\omega_1/v,\omega_1)\left[\frac{\omega_1 \ell e}{mv^3}\ E(\omega_2/v,\omega_2)\right]\frac{\partial f_o}{\partial v}$$

$$\times\ \exp[-\tilde{D}_{33}\omega_1^2\ \omega_2 \ell^3 \,/\, 3v^5]\Big|_{v=\omega_3/k} \qquad (20a)$$

The importance of (20a) is that a given k corresponds to a particular velocity ω_3/k in $G(v,\ell)$, so that one can observe the contribution of electrons of a given velocity to the echo as a function of ℓ. The only dependence of G on ℓ in (18), except for an overall factor of ℓ which can be divided out of the experimental data, is in the damping terms, which have been combined to give

$$D = \exp\left[-\frac{\ell^3\omega_1^2\ \omega_2\ \tilde{D}_{33}(v)}{\omega_2 3v^5}\right] \quad \text{, as obtained by O'Neil [18] .} \qquad (20b)$$

By recording the echo amplitude $\hat{E}(z-\ell')$ for several ℓ values and Fourier transforming it to give $\hat{E}(k)$, one can obtain $D_{33}(v)$ over some range of v. This can be accomplished in practice by changing z at a constant rate and taking digital samples of $E(z-\ell')$ at a fixed frequency. The digital information can then be Fourier analyzed on a computer. Furthermore, one does not have to know the dependence of $G(v,\ell)$ on v, because one run (one ℓ value) can be used to divide it out after the transform has been taken.

The one weakness of this method is its evaluation of the damping at the center of the echo, while in fact the damping is changing over the width of the echo. In this experiment $(z-\ell')^3$ does change

significantly over the echo width, but the Fourier transforming of the experimental results still yields good agreement with the ℓ^3 damping dependence. That fact, plus the complexity of an exact analysis, lead the author to make no further improvement in that part of the theory.

1.4 Echo Saturation

In Section 1.3 a perturbation expansion in the applied fields was used to calculate the echo electric field. It is also possible to consider the motion of individual electrons to obtain the echo, without using the Vlasov equation, in the absence of collisions. One finds (Coste and Peyraud [11] that the echo amplitude saturates with increasing amplitude of the signal on the second exciter, or for a fixed amplitude, with increasing ℓ . The saturation effects could therefore be confused with damping and are to be avoided.

The perturbed distribution function by this method is obtained from (8), Appendix 1, as

$$f_1(x,v,\omega_3) = \frac{e}{mv}\mathcal{E}_1 J_1\left(\frac{\omega_1 e \mathcal{E}_2}{v^3 m}\right)\frac{\partial f_o}{\partial v}$$

$$\times i \exp[i(\theta_2 - \theta_1) + i(\omega_2(x-\ell) - \omega_1 x)/v] \qquad (21)$$

Rewriting (18) without damping and with F written out, one has

$$f_1(x,v,\omega_3) = i\frac{\omega_1 \ell}{2v^4}\left(\frac{e}{m}\right)^2 \frac{\partial f_o}{\partial v}\hat{E}(\omega_2/v,\omega_2)\hat{E}^*(\omega_1,\omega_1/v)$$

$$\times \exp[i(\omega_3 x - \omega_2 \ell)/v] \quad . \qquad (22)$$

When the argument of J_1 is sufficiently small, (21) and (22)

agree. The echo electric field due to (21) is

$$\tilde{E}(k\omega_3) = \mathrm{Re}\ \frac{2\pi e}{k^2\,(\omega_3,k)\mathcal{E}_o}\,\frac{e}{m}\,\mathcal{E}_1 J_1\!\left(\frac{\omega_1 e \ell}{m v^3}\,2\right)\frac{\partial f_o}{\partial v}\,e^{i(\theta_2-\theta_1)}\Bigg|_{v=\omega_3/k}.$$

The most interesting feature of (21) is that for a given v, for a sufficiently large $\mathcal{E}_2$, the contribution to the echo by electrons of velocity v will decrease to zero. To observe this experimentally, it is necessary to isolate a single velocity, for if there is any spread, the integral over all the velocities will not approach zero as J_1.

As in Section 1.3, a given wave number k corresponds to a velocity ω_3/k. One can observe the Bessel function behavior experimentally by fixing ℓ and taking a series of runs with varying amplitudes on the second exciter. The Fourier transform of the echo amplitude then gives the echo amplitude as a function of velocity.

It is then possible to compare the amplitude curve for a given v with J_1, and fitting J_1 to the curve, obtain its argument as a function of v. Unfortunately, it will not vary just as $1/v^3$, because $\mathcal{E}_2$ is a function of wave number and therefore of v.

If one chooses an exciting field of the form $E = 0$ for $x < -h$ or $x > h$, $E = \mathcal{E}_o \cos \omega t$ for $-h \le x < 0$, and $E = -\mathcal{E}_o \cos \omega t$ for $0 < x \le h$, then $\hat{E}(k,\omega) = i\frac{\mathcal{E}_o}{k}(2 - 2\cos kh)$. If h is taken as the Debye length (.05 cm in this experiment), and k is taken as ω/v (typically 15 cm^{-1}), $hk \simeq .75$. That is really a minimum value of hk, so that one cannot use a small argument approximation for $\cos(x)$. In the chapter on experimental results, a comparison of the data with $(1 - \cos(h\omega_2/v))/v^2$ is made.

The experimental results also show that the damping experiments were done at amplitudes at which J_1 is quite linear. It is fortunate that the series for $J_1(x)$ starts as $(x/2)(1 - x^2/8 + \cdots)$, so that J_1 is linear for relatively large valued x .

1.5 The Coefficient of Diffusion in Velocity Space

The diffusion tensor is defined as

$$D_{ij} = \lim_{\Delta t \to 0} \frac{1}{2} \frac{\langle \Delta v_i \, \Delta v_j \rangle}{\Delta t} \tag{23}$$

where Δv is the change in velocity an electron undergoes in time Δt due to the fluctuating electric field of the cloud of electrons surrounding it. In order to apply a continuous stochastic theory to what is microscopically a discontinuous process, Δt must actually remain large compared to the correlation time of the fluctuating fields. Simultaneously, it must be small compared to macroscopic times.

From $\dot{\vec{v}} = \frac{e}{m}(\vec{E}(\vec{R}(t),t) + \vec{v} \times \vec{B}_o)$, where $\vec{v} = \dot{\vec{R}}$, one obtains

$$\Delta v_z = \frac{e}{m} \int_t^{t+\Delta t} E_z(\vec{R}(t'),t') \, dt' \tag{24}$$

if B_o is in the z direction. The first order approximation in the field is

$$\Delta v_z \simeq \frac{e}{m} \int_t^{t+\Delta t} E_z(\vec{R}_o(t'),t) \, dt' \tag{25}$$

where

$$\vec{R}_{o\perp}(t) = \vec{r}_{o\perp} - \frac{M}{\omega_c}[\exp(M\omega_c t) - I] \, \vec{v}_{o\perp} \tag{5c}$$

$$\vec{R}_{o\parallel}(t) = Z_o(t) = z_o + v_{o\parallel} t \tag{5a}$$

Then from (23)

$$D_{33} = \frac{1}{2}\left(\frac{e}{m}\right)^2 \int_t^{t+\Delta t}\int_t^{t+\Delta t} \frac{\langle E_z(\vec{R}_o(t'),t')\, E_z(\vec{R}_o(t''),t'')\, dt'dt''\rangle}{\Delta t}$$

$$= \frac{1}{2}\left(\frac{e}{m}\right)^2 \int_t^{t+\Delta t} \langle E_t(\vec{R}_o(t'),t')\, E_z(\vec{R}_o(t+\xi),t+\xi)\rangle\, dt' \qquad (26)$$

for some ξ in the interval $[t,t+\Delta t]$.

Because Δt is assumed large compared to the correlation time of the field, (26) is approximately

$$D_{33} \simeq \frac{1}{2}\left(\frac{e}{m}\right)^2 \int_{-\infty}^{\infty} \langle E_z(\vec{R}_o(t-t'),t-t')\, E_z(\vec{R}_o(t),t)\rangle\, dt' \quad . \qquad (27)$$

Upon taking the spatial and temporal Fourier transforms of the fields, one obtains

$$D_{33} \simeq \frac{1}{2}\left(\frac{e}{m}\right)^2 \iiint \langle E_z^2\rangle_{\omega,\vec{k}} \exp[ik\cdot(\vec{R}_o(t) - \vec{R}_o(t-t')$$

$$- i\omega t']\, \frac{d^3k\, d\omega\, dt'}{(2\pi)^4}$$

In the experimental case of interest, the electron Larmour radius is considerably smaller than a Debye length, so that the assumption of an infinite B_o is a reasonable first approximation. Therefore,

$$\vec{R}_{o\perp} \simeq \vec{r}_{o\perp} \qquad \text{and} \qquad \vec{R}_{o\perp}(t) = z_o + v_{o\parallel}t \quad , \quad \text{so that}$$

$$D_{33} \simeq \frac{1}{2}\left(\frac{e}{m}\right)^2 \iiint \langle E_z^2\rangle_{\omega,\vec{k}} \exp[i(k_z v_{o\parallel} - \omega)t'] \frac{d^3k\, d\omega\, dt'}{(2\pi)^4}$$

$$= \frac{1}{2}\left(\frac{e}{m}\right)^2 \int_{-\infty}^{\infty}\int \langle E_z^2\rangle_{\omega,k_z} \delta(k_z v_{o\parallel} - \omega) \frac{dk_z\, d\omega}{2\pi}$$

$$= \frac{1}{2}\left(\frac{e}{m}\right)^2 \int_{-\infty}^{\infty} \langle E_z^2\rangle_{v_{o\parallel}k_z,k_z} \frac{dk_z}{2\pi} \qquad (28)$$

where $\langle E_z^2\rangle_{\omega,k_z} = \iint_{-\infty}^{\infty} \langle E_z^2\rangle_{\omega,\vec{k}} \frac{d^2k}{(2\pi)^2}$.

From the fluctuation-dissipation theorem (Sitenko [24],p.28), one has

$$\langle E_z^2\rangle_{\omega,\vec{k}} = \frac{4\pi i\, \kappa T}{\omega} \{\Lambda_{33}^{-1} - \Lambda_{33}^{-1*}\} \qquad (29)$$

where $\Lambda_{ij}(\omega,\vec{k}) = \eta^2\left(\frac{k_i k_j}{k^2} - \delta_{ij}\right) + \varepsilon_{ij}(\omega,\vec{k})$ and $\eta = kc/\omega >> 1$.

For an infinite $\vec{B}_o$, the plasma dielectric function ε_{ij} becomes

$$\begin{pmatrix} 1 & 0 & 0 \\ 0 & 1 & 0 \\ 0 & 0 & \varepsilon_\ell \end{pmatrix} .$$

$$\Lambda_{33}^{-1} = \frac{1 - \eta^2 k_\parallel^2/k^2}{\varepsilon_\ell - \eta^2(k_\parallel^2\varepsilon_\ell + k_\perp^2)/k^2} \quad , \text{ where}$$

$k_\parallel = k_z$, and $k_\perp^2 = k_x^2 + k_y^2$. For $\eta >> 1$, this becomes

$$\Lambda_{33}^{-1} \simeq k_\parallel^2 / (k_\parallel^2\varepsilon_\ell + k_\perp^2) .$$

From (29) we then obtain

$$\int\int \langle E_z^2 \rangle_{\omega,\vec{k}} \frac{d^2k}{(2\pi)^2} = -\frac{2\kappa T}{\pi\omega} \operatorname{Im} \int_0^\infty \int_0^{2\pi} \frac{k_{\parallel}^2 \, d\theta k_\perp dk_\perp}{k_\perp^2 + \varepsilon_\ell k_{\parallel}^2}$$

$$= \frac{2\kappa T}{\omega} k_{\parallel}^2 \tan^{-1} \left[\frac{\operatorname{Im} \varepsilon_\ell}{\operatorname{Re} \varepsilon_\ell}\right] \quad . \tag{30}$$

From Sitenko [24], p.41, $\varepsilon_\ell = 1 + (1 - \phi(z) + i\sqrt{\pi}\, z \exp[-z^2])/a^2k^2$, where $z = \omega/k_{\parallel}v_e = v_{o\parallel}/v_e$, $v_e = \sqrt{\frac{2\kappa T}{m_e}}$, $a = \frac{v_e}{\sqrt{2}\,\omega_p}$ is the Debye length, and $\phi(z) = 2z \int_0^z \exp[x^2 - z^2]dx$.

Substitution of this into (28) gives

$$D_{33} = \frac{2\kappa T (e/m)^2}{v_o} \int_0^{k_o} k_{\parallel} \tan^{-1}\left[\frac{\sqrt{\pi}\, z \exp[-z^2]}{a^2k_{\parallel}^2 + (1 - \phi(z))}\right] \frac{dk_{\parallel}}{2\pi} \tag{31}$$

where k_o cuts off the integration at impact parameters for which binary collisions are important, namely $1/k_o = e^2/mv_e^2$. Typical values of $\ell n(ak_o)$ are given in Spitzer [25], p.73.

Letting $A = \sqrt{\pi}\, z\, e^{-z^2}$, $B = 1 - \phi(z)$, one obtains upon integrating (31),

$$D_{33} = -\frac{\kappa T}{2\pi} \frac{(e/m)^2}{a^2 v_{o\parallel}} \left\{ -\frac{\tan^{-1} uA}{u} - \frac{A}{2} \log \frac{1/A^2 + u^2}{u^2} \right\} \Bigg|_{1/B}^{1/(ak_o)^2}$$

$$\simeq \frac{\kappa T}{2\pi} \frac{(e/m)^2}{a^2 v_{o\parallel}} A \left\{2\, \ell n(ak_o) - \ell n\, A\right\} \quad . \tag{32}$$

$$\simeq \frac{e^2}{m} \frac{\omega_p^2}{v_{o\parallel}} \ell n\, ak_o \frac{A}{\pi}$$

This can be compared with the isotropic case, where the coefficient of diffusion in the direction of particle motion is

$$D_{\parallel} = \frac{e^2 \omega_p^2}{m v_{o\parallel}} \ell n(ak_o)\ G(v_{o\parallel}/v_e) \quad , \tag{33}$$

where $G(\zeta) = [\mathrm{erf}(\zeta) - \zeta\ \mathrm{erf}'(\zeta)]\ /2\zeta^2$ (Sitenko [24], p.142).

In the experimental case of interest, $\ell n\ ak_o \simeq 13$.

In Section 3.2, these two diffusion coefficients are compared with the experimental results.

In reality, the electron neutral collisions are not negligible compared to Coulomb collisions. However, the electron neutral collisions are qualitatively different from the Coulomb collisions. While the interaction between the test electron and any electron in general has a negligible effect on the test electron, the electron neutral collisions are individually effective in completely changing the electron motion. Therefore, the electron neutral collisions do not represent a diffusion process, so that the effect on electrons of velocity v contributing to the echo is to reduce the echo amplitude by $\exp[-\ell'/\lambda(v)]$, where $\lambda(v)$ is the mean free path of electrons of velocity v in that gas, and ℓ' is the distance from the first exciter to the echo. Although it is true that electrons of some velocity v' will be scattered into velocity v, they will have a random phase with respect to the echo, so contribute nothing.

The quantity $\lambda(v)$ has been experimentally determined (Brode [26]). This correction has been applied to transformed experimental data as a function of velocity using the measured neutral gas pressure. This correction only has a slight effect on the ℓ-dependence of the damping

mainly at small ℓ values, because the Coulomb collisions rapidly become dominant for large ℓ values.

II. EXPERIMENTAL APPARATUS AND DIAGNOSTICS

2.1 The Vacuum System and Plasma Generator

The plasma source is shown schematically in Figure 1. The vacuum vessel consists of a piece of 6-inch inside diameter pyrex pipe 5 feet long. One end joins a reducing elbow connected to a throttle valve, a 4-inch refrigerated cold trap and a 4-inch diffusion pump using hydrocarbon oil. At the opposite end of the pipe is a stainless steel plate to which are attached three vacuum motion feed-throughs, a low power electrical feed-through, and four high current and water feed-throughs.

The plasma is surrounded by a 10 cm diameter slotted stainless steel cylinder. It is terminated on the diffusion pump end by a graphite (to reduce secondary emission) collector at the cylinder potential which is the accelerating grid of the electron gun. The control grid and cathode follow. The grids are made of .001 inch tungsten wire spaced 100 wires to the inch.

The electron emitter is an indirectly heated oxide coated cathode. The emitting surface is made by spraying Eimac #422 solution onto a two-inch diameter, one-eighth inch thick nickel disk which can be detached from the rest of the gun assembly. This disk is radiantly heated by a self-supporting bifilar spiral made of .080 inch tungsten wire which is surrounded by three nested heat shields. In operation the heater requires three volts at forty amperes. The cathode and heater structure is backed by and attached to a copper plate, to which is attached one heater wire. The heater current is carried through the

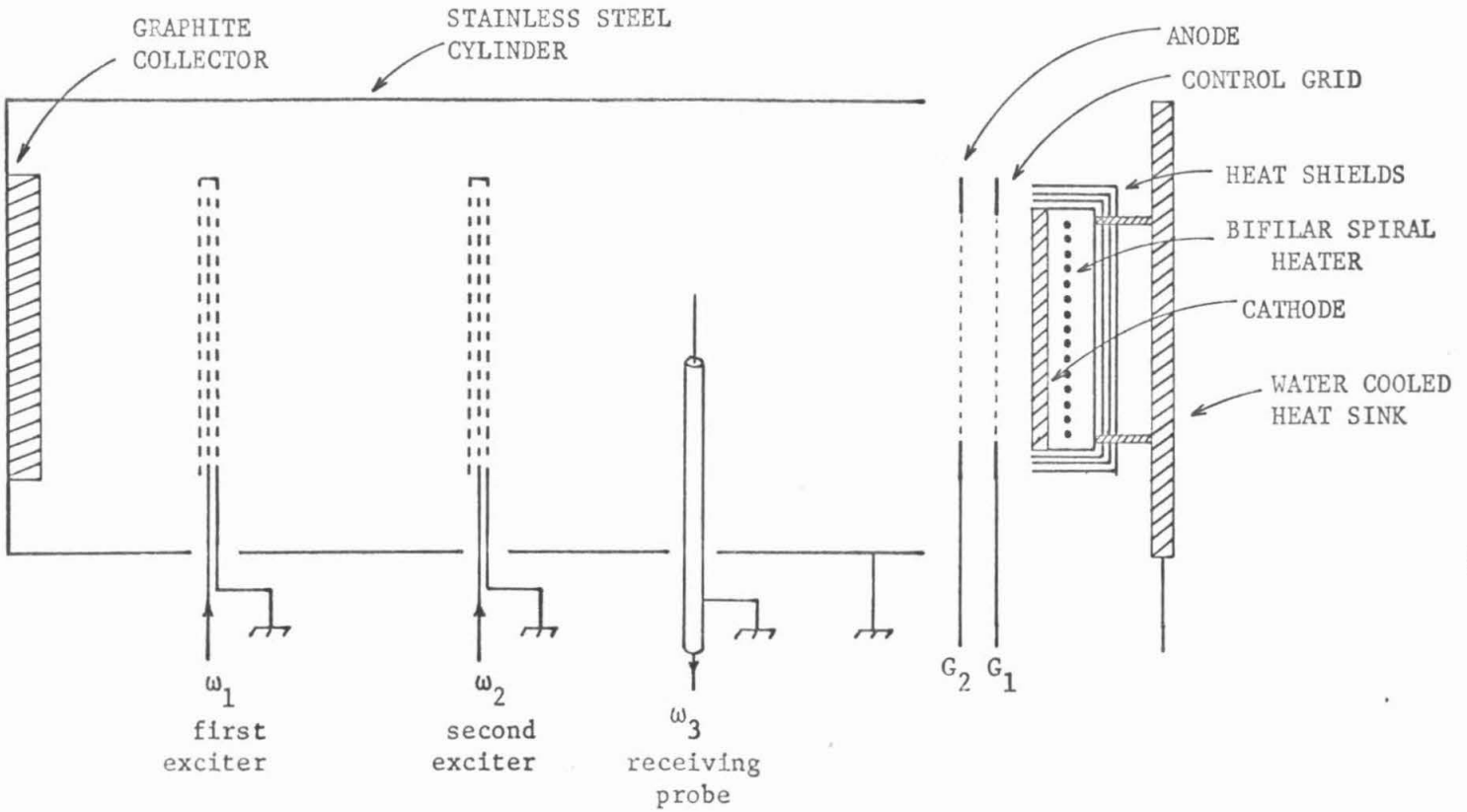

Fig. 1. Plasma Source

vacuum seals by two pairs of copper tubes forming two loops inside the system. One loop is attached to the copper mounting plate while the other is attached to the other heater wire. Water circulating through the loops keeps most of the structure cool, which reduces out-gassing, and permits the use of simple O-ring vacuum seals in place of the ceramic feed-throughs which would otherwise be required.

The author initially found that after the cathode had been off for some time and was turned on it failed to emit. It was observed upon removing the cathode from the system that it was coated with a dull black substance, which was taken to be decomposed hydrocarbons. It was difficult to remove all sources of hydrocarbons because of all the sliding probes in the system which needed lubrication. Silicon compounds had been found by others in the laboratory to be even worse, for they caused silicon oxide to form on cathodes. The solution was found to be to maintain a low voltage argon glow discharge in the system when it was not in operation. Once this procedure was started, the same cathode coating was used for the remainder of the experiment, with little reduction in emission. The cathode with one coating and the original heater remained in operation continuously for 3500 hours, at which time it was turned off because the experiment was completed. Presumably sputtering kept the cathode surface clean.

The stainless steel cylinder is electrically connected to the vacuum system end plate which is at ground potential, while the cathode is operated at -400 volts with respect to the cylinder.

A feedback system is used to maintain a constant current passing through the accelerating grid.

All the current collected by the cylinder and its end plate plus that collected by all other electrodes in the plasma other than the accelerating grid G2 is sensed by a control device, which compares it to a standard and sets the control grid G1 voltage accordingly. In order to avoid amplifying noise in the plasma, the feedback path contains an integrator, which gives the device a long time constant.

Two grids and a probe could move independently of each other on a set of tracks under the axially slotted cylinder and the cathode. Three long 1/4 inch tubes each carrying a vacuum sealed rigid coaxial cable could move through a vacuum motion feed-through. Inside the system each tube was attached to a nylon runner on one of the tracks. The coaxial cable came up through the runner, through the axial slots in the cylinder to connect to and support a grid or probe.

The two grids actually each consisted of three planar grids, each three inches in diameter. The two outer grids were connected to the outer coaxial conductor, while the middle grid was connected to the inner conductor of the coax. Each grid consisted of a machined copper ring on which .001 tungsten wire was wound to form a "cheese cutter". There were 30 wires to the inch, so that three grids were still at least 90% transparent. The rings were all machined identically so that the corresponding wires of the three grids were aligned.

The probe was a .01 inch diameter tungsten wire sheathed with glass except for a one cm length. The center of the exposed wire then approximately intersected the axis of symmetry of the cylinder.

2.2 General Discussion of the Beam Produced Plasma

The plasma used in this experiment was produced by a large diameter beam of high energy electrons passing through argon parallel to a uniform confining 1 kilogauss magnetic field.

Beam produced plasmas have been described by Dunn et al [27] and Hirose et al [28].

It has been found that under proper operating conditions a beam can produce a very low noise, low temperature plasma in a magnetic field. For a given gas pressure and beam energy, as the beam current is increased, the plasma will shift discontinuously from a stable mode confined to the beam diameter to an unstable mode spreading to the container walls.

In the stable mode it was found by Dunn [27] that the beam energy remains essentially monoenergetic, so that the electron velocity distribution consists of two parts, one falling off rapidly with increasing beam energy, and the other a spike at the beam potential. Also, the density of the beam is generally several orders of magnitude lower than that of the plasma, so that the beam does not have to be considered in the distribution function of the plasma, provided one is well into the stable mode.

Besides low temperature and low noise, the beam produced plasma has the advantage that there is no potential drop along the column. As is shown in Figure 1, the beam is accelerated by a fine mesh anode near the thermionic cathode and collected by a plate at the anode potential at the opposite end of the column. Also, the plasma is produced uniformly throughout its volume, and because the beam electrons are not

affected by sheaths, electrodes in the plasma do not cast large shadows.

The high energy beam electrons do have the disadvantage that they produce secondary emission from some surfaces. This could alter the distribution function for electrons in a non-reproduceable way because secondary emission from metal surfaces can depend on thin oxide films, which could change with time. It was found that several hours were required after starting the discharge for the echo shape to stabilize; even though the density, gas pressure, beam voltage, and beam current remained constant. The change in the echo shape during this time suggested a gradual diminution of the number of low energy electrons.

Another undesirable feature of a beam produced plasma is its ability to act as an amplifier. Although the gain at a given frequency depends on many factors, such as the perveance of the electron gun, the plasma density, and column diameter (which have been analyzed by Self [29]), it appears that the gain falls off rapidly for frequencies above the plasma frequency. Indeed, the stability of the plasma is determined by the requirement that the attenuation of any wave travelling upstream be greater than the gain of the beam plasma amplifier. Instabilities aside, it would be highly undesirable in this experiment to have applied signals amplified by the plasma. All the work has therefore been done with the receiving probe upstream from any exciters.

2.3 Plasma Diagnostics and Parameters

The properties of the plasma used in this experiment were studied by the use of D.C. probes, propagation of ion acoustic waves, and excitation of plasma resonance cones.

The D.C. probes were used to plot the radial density profile and axial density uniformity and to find the operating conditions which gave the lowest noise and lowest electron temperature. A port in the side of the vacuum vessel allowed a probe to move radially in a region near the electron gun, while the probe used as the receiver of RF signals was used to observe noise, temperature, and axial density uniformity.

The radial density profile, measured by drawing ion current with a probe biased at -45 volts with respect to the anode, is shown in Figure 4a. Over the 12-inch travel of the receiving probe, the ion saturation current (which never really saturated) fell by 5% from its high central value to its value near the electron gun.

In order to observe the desired echo phenomena, it is necessary to have a low temperature and low noise. For purposes of finding the optimum operating conditions, a Langmuir probe display unit was designed and constructed similar in concept to one described by Harp [30]. The device applies a sawtooth voltage to the probe and displays the logarithm of the current on one channel of a dual trace oscilloscope. The other channel is driven by an adjustable slope sawtooth from the unit which is calibrated in electron temperature. One then adjusts the slope of the calibrated sawtooth to equal that of the probe current. Because the ion current drawn by a cylindrical probe in a magnetic field does not saturate, there is some ambiguity in subtracting the ion current before taking the logarithm, but it is extremely convenient for observing relative changes in the electron distribution function.

It was found that the lowest temperature was obtained with the background argon pressure at 1.6×10^{-3} torr, the total beam current at

.3 ma, and the beam accelerating voltage at 400V. Using a true RMS voltmeter to observe the ion current noise with the probe biased at -45V with respect to the surrounding metal cylinder, the ratio of the RMS to D.C. currents was less than 0.5%, with frequencies up to 5 MHz included.

Ion acoustic waves were used to measure the electron temperature. From the dielectric function (Gould [3]) for a Maxwellian plasma:

$$K(\omega,k) = 1 - \frac{\omega_{pi}^2}{k^2 v_i^2} Z'(\frac{\omega}{kv_i}) - \frac{\omega_{pe}^2}{k^2 v_e^2} Z'(\frac{\omega}{kv_e})$$

where $v_e = \sqrt{\frac{2\kappa T_e}{m_e}}$, $v_i = \sqrt{\frac{2\kappa T_i}{m_i}}$, T_e and T_i are the electron and ion temperatures, κ is Boltzmann's constant, ω_{pe} and ω_{pi} are the electron and ion plasma frequencies, and Z' is the derivative of the plasma dispersion function (Fried and Conte [26]). For cold ions and long wavelengths, $v_i << \frac{\omega}{k} << v_e$. For large arguments,

$$Z'(\zeta) = -2\zeta i\sqrt{\pi} e^{-\zeta^2} + \frac{1}{\zeta^2} + \frac{1}{\zeta^3} + \cdots \quad \text{, asymptotically,}$$

while for small arguments

$$Z'(\zeta) = -2\zeta\, i\sqrt{\pi} e^{-\zeta^2} - 2 + \frac{8}{3}\zeta^2 - \frac{32\zeta^4}{15} + \cdots .$$

$$K(\omega,k) \simeq -\frac{m_e}{m_i}\frac{\omega_{pe}^2}{k^2 v_i^2}(\frac{k^2 v_i^2}{\omega^2}) - \frac{\omega_{pe}^2}{k^2 v_e^2}(-2)$$

if one ignores Landau damping (the imaginary terms), and with m_e and m_i the electron and ion masses and neutrality assumed. Then,

$$K(\omega,k) = -\frac{m_e}{m_i}\frac{\omega_{pe}^2}{\zeta^2} - \frac{\omega_{pe}^2}{k^2 v_e^2}(-2) \quad .$$

The dispersion relation is given by $K(\omega,k) = 0$, which gives

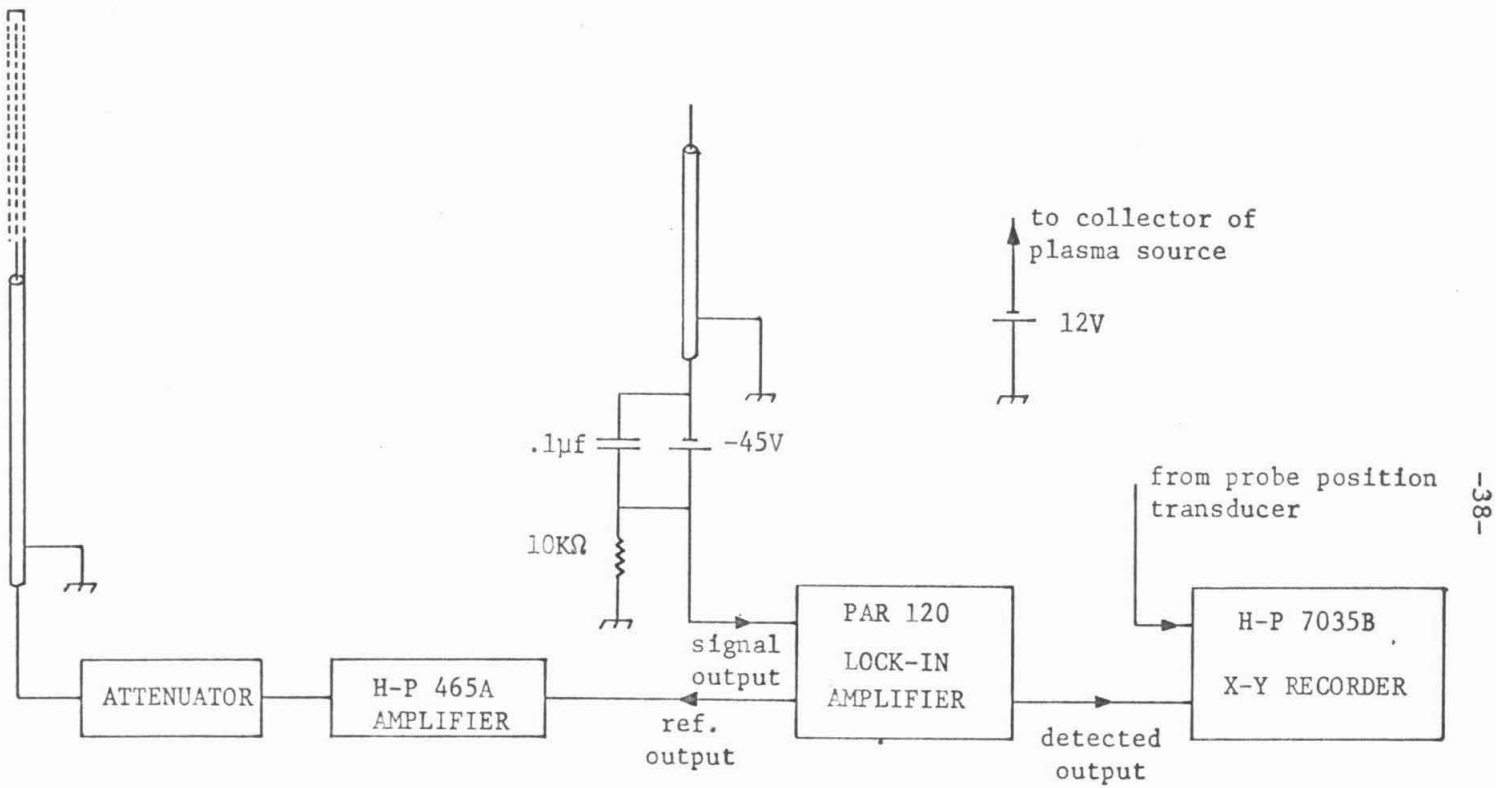

Fig. 2. Ion Wave Set-Up

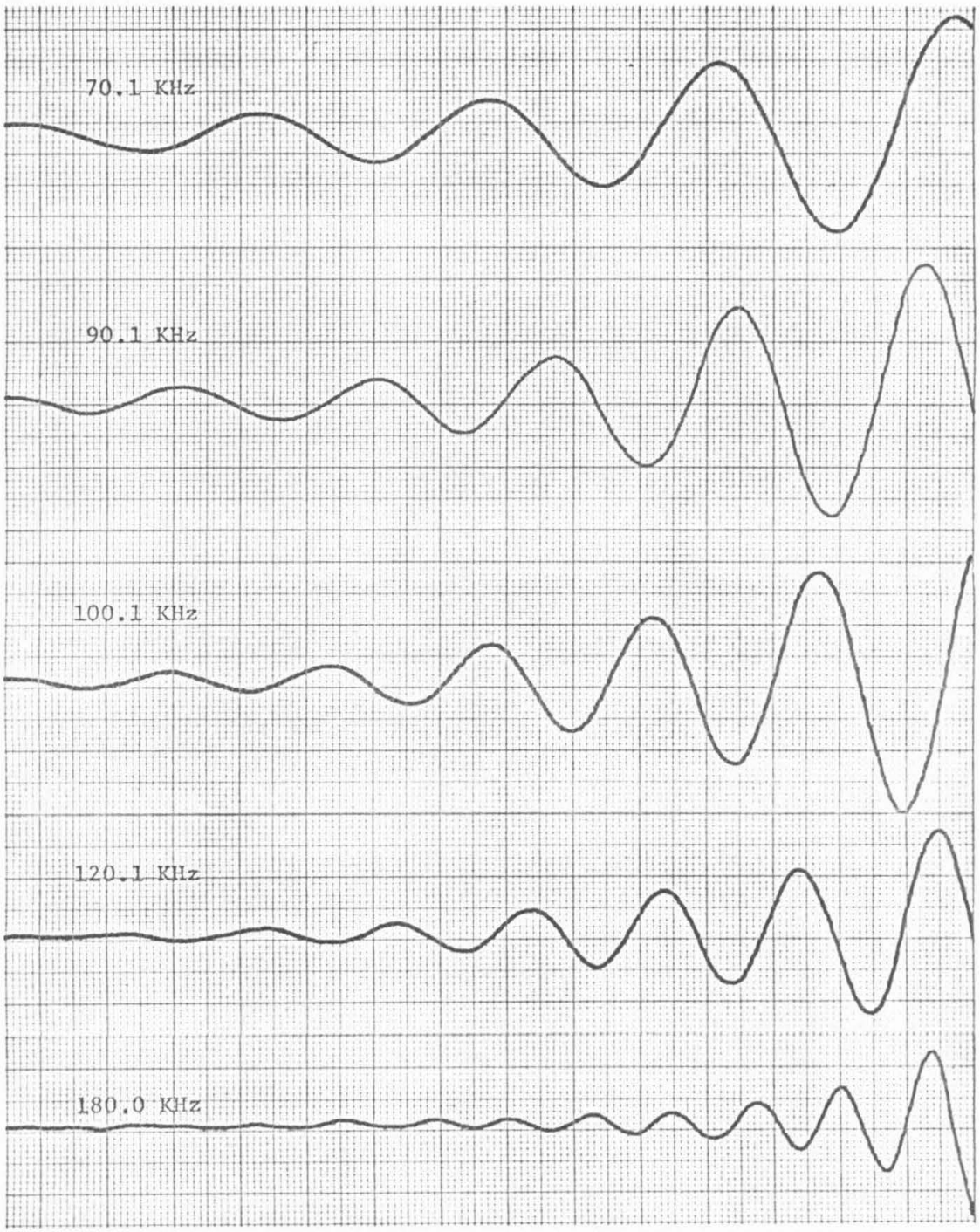

1 cm = .5 cm in apparatus

Fig. 3. Sample of ion waves for various frequencies.

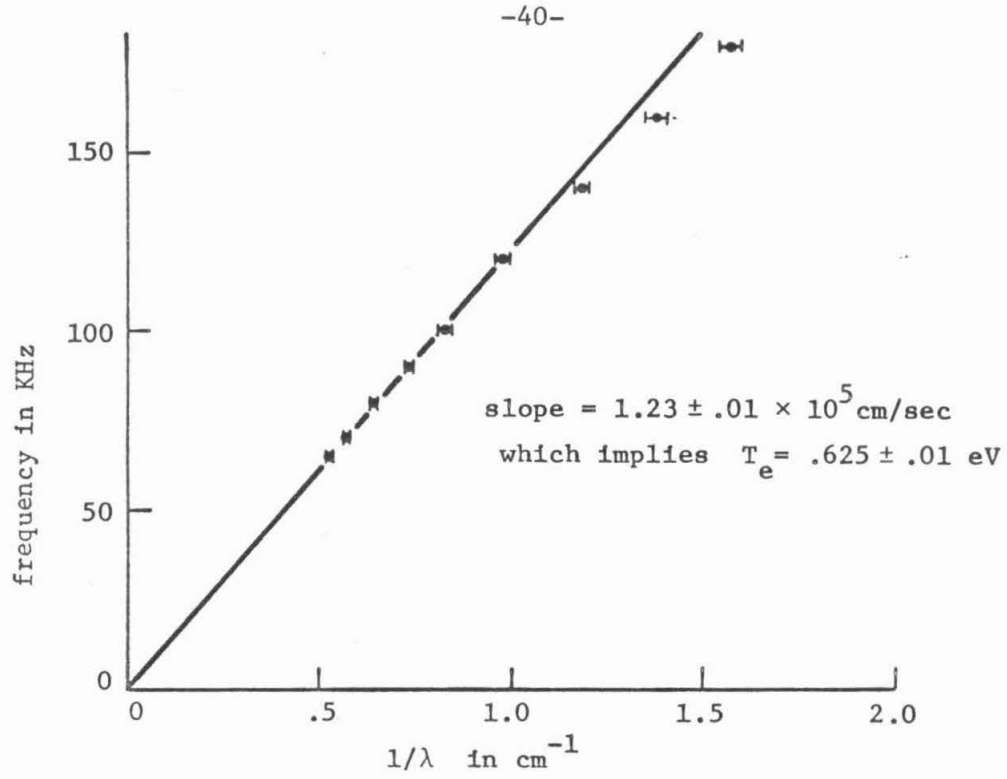

Fig. 4b. Dispersion of ion-acoustic waves

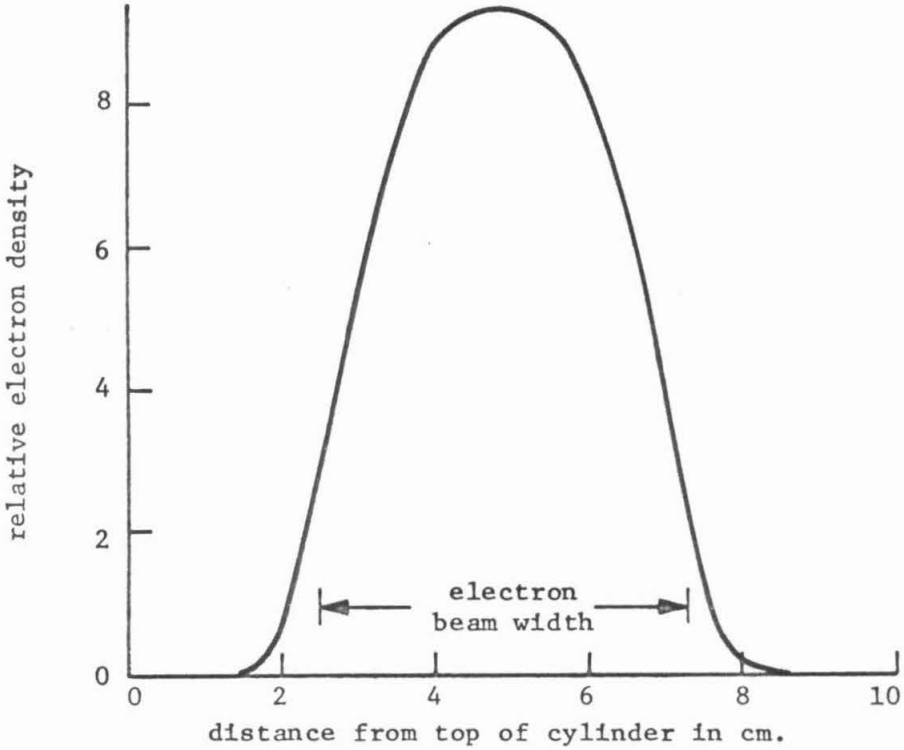

Fig. 4a. Electron density profile

$$v_e^2 = \frac{2\omega^2}{k^2}\frac{m_i}{m_e}$$

Thus if one works in a region where ω/k remains constant with frequency, one can measure the temperature. The experimental arrangement is shown schematically in Figure 2. The applied voltage on the exciting grid is about 0.1 volts peak. The system is an interferometer arrangement, so that by moving the receiving probe, one can determine the wave number.

The traces obtained on an X-Y recorder with the X voltage proportional to the probe position for various frequencies are shown in Figure 3 for the usual plasma conditions. The waves are damped in part because of ion-neutral collisions. The experimentally determined dispersion shown in Figure 4b yields an electron temperature of about 0.65 eV. The probe display system gave $1.0 \pm .4$ eV, the uncertainty due to the choice of ion saturation current.

Although for a Maxwellian plasma the ion waves should give the correct value, in the more usual non-Maxwellian case, the temperature given involves an average which is insensitive to the high energy tail of the distribution. This can be seen from the dielectric function, which has the integral form

$$K(\omega,\vec{k}) = 1 - \frac{\omega_{pi}^2}{k^2}\int \frac{\vec{k}\cdot\nabla_v f_i(\vec{V})}{\omega - \vec{k}\cdot\vec{V}}\, d^3V - \frac{\omega_{pe}^2}{k^2}\int \frac{\vec{k}\cdot\nabla_v f_e(\vec{V})}{\omega - \vec{k}\cdot\vec{V}}\, d^3V$$

where f_i and f_e are the ion and electron distribution functions. In the second integral $\omega/k << \vec{V}_e$, so that this integral is approximately

$$+ \frac{\omega_{p_e}^2}{k^2}\int \frac{\partial[f_e(v)]}{\partial v^2}\, dv \quad \text{in one dimension.}$$

To see the effect of this average, let $f_e(v)$ be a piecewise smooth combination of two Maxwellians of temperatures T_1 and T_2, joined at velocity V_c. In the case of a central distribution of $T_1 = .5$ eV and a tail of $T_2 = 3$ eV, joined at $V_c = 5 \times 10^7$ cm/sec, one would obtain an experimental electron temperature of .66 eV. Therefore, the ion-waves are not at all sensitive to high energy tails, even though the tail would contain 30% of the electrons in this case.

For comparisons with theory, the electron density n_e is also an important quantity. Unfortunately, for low densities, its measurement in a magnetic field is difficult. Electromagnetic resonances at microwave frequencies involving the dielectric function perpendicular to the magnetic field will work in principle, but the precision at $\omega_{pe} \sim 100$ MHz makes them useless. The resonance cone technique (Fisher and Gould [32]) can still be useful at such low plasma frequencies, however.

Following reference 32, in the near field region of a radiating probe one need consider only the electrostatic part of Maxwell's equations. For a cold, uniform magnetoplasma with stationary ions, the dielectric tensor K is diagonal and is given by $K_{xx} = K_{yy} \equiv K_\perp = 1 - \omega_p^2/(\omega^2 - \omega_c^2)$ and $K_{zz} = K_{\parallel} = 1 - \omega_p^2/\omega^2$, where ω_c and ω_p are the electron cyclotron and plasma frequencies, respectively, and the magnetic field is in the z direction. The potential due to an oscillating point charge is then, in cylindrical coordinates

$$\phi(\rho,z) = \frac{q\, e^{-i\omega t}}{4\pi\varepsilon_o (K^2 K_{\parallel})^{1/2} \left[\rho^2/K_{\perp} + z^2/K_{\parallel}\right]^{1/2}}$$

A resonance will occur when $(\rho/z)^2 = \tan^2\theta = -K_{\perp}/K_{\parallel}$.

$$\tan^2\theta = -\frac{1 - \omega_p^2/(\omega^2 - \omega_c^2)}{1 - \omega_p^2/\omega^2} \cong -\frac{1}{1 - \omega_p^2/\omega^2}$$

for large magnetic fields. One then obtains $\sin^2\theta = \omega^2/\omega_p^2$.

In a warm plasma in the presence of collisions or with exciters of non-zero dimensions, the infinity is replaced by a maximum. Indeed, with the small probe separation possible in this experiment, the maxima were inconveniently broad.

A pair of probes with a 2 cm separation which could rotate about a common axis were installed in the system in place of the radially moving probe. The axis of rotation was then perpendicular to the magnetic field. At a frequency of 50 MHz, the cone angle was observed to be 32 ± 2 degree, which implies $\omega_p = 94 \pm 6$ MHz, and $n_e = 1.1 \pm .15 \times 10^8/cm^3$.

2.4 The Receiving System

The receiving system consisted of 3 stages of R.F. amplification at the echo frequency followed by a balanced mixer. The local oscillator signal for the mixer was generated coherently from the two signals used to generate the echo. One of these transmitting signals was A.M. modulated at 1 KHz by a reference signal from a lock-in amplifier before being applied to the plasma. The output of the balanced mixer was then a 1 KHz signal which was the input for the lock-in amplifier.

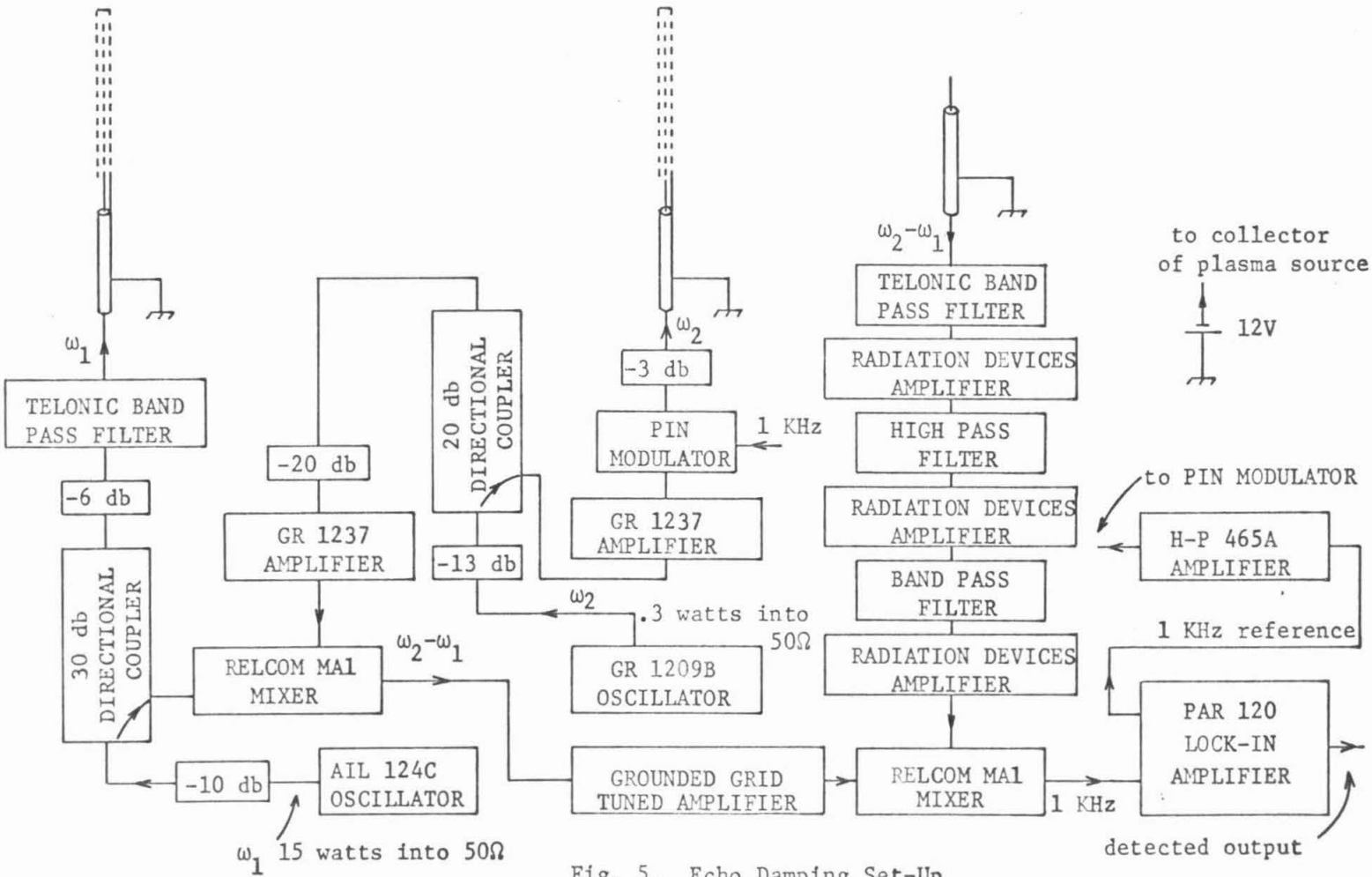

Fig. 5. Echo Damping Set-Up

The input to the receiver was always a tuned bandpass filter which was intended to protect the following broad band amplifier from excessive noise. The amplifiers were three Radiation Devices Co. model BBA-1P broad band amplifiers which, at the typical 250 MHz operating frequency each had a gain of 23 db and a noise figure of 3 db. It unfortunately proved necessary to put high pass filters between stages to prevent low frequency oscillation between amplifiers. Assuming total filter losses at 6 db and mixer losses at 7 db, the overall gain up to the lock-in amplifier input was 56 db. The Princeton Applied Research model 120 lock-in amplifier was usually operated on its most sensitive .1 mV full scale input. The output was usually less than one-tenth full scale, however, so that the RF input to the receiver was less than 56 db below 10 microvolts or about 10^{-8} volts. It was not practical to increase the applied signals to the plasma because saturation effects would have become important.

With that low a signal level considerable effort was required to prevent the RF reference signal at the echo frequency from becoming modulated and entering the receiver. Even with the precautions taken, there were unwanted signals which changed erratically as the probe moved and resulted in apparent noise. It proved necessary to drive the probe at about 1 cm/min to permit sufficient low pass filtering of the lock-in amplifier output to obtain a reasonable trace.

Two different configurations were used for generating the RF reference signal and the signals to the plasma: one for observing the echo damping and one to observe saturation of the echo amplitude.

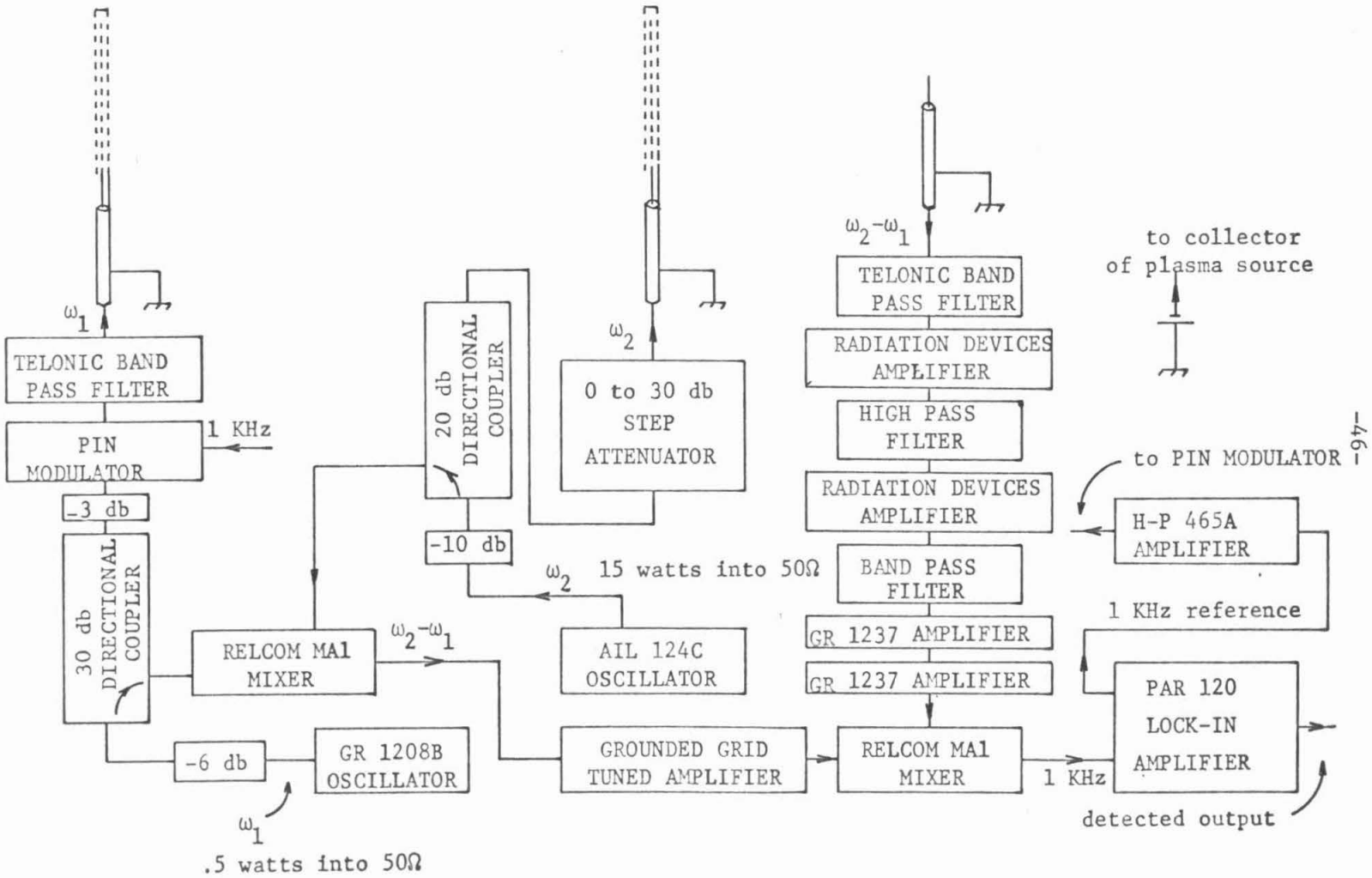

Fig. 6. Echo Saturation Set-Up

The arrangement to observe echo damping is shown in Figure 5. Referring to that figure, the purpose of the two directional couplers and two General Radio amplifiers is to isolate the RF reference signal from the grid 1 and grid sources. One wishes to avoid either having the reference signal modulated at 1 KHz or having this signal appear at either grid. The vacuum tube tuned amplifier, which was built by the author, consists of three tuned grounded grid stages. It has a gain of about 20 db over a tunable range of 125 to 280 MHz. Aside from acting as a tuned filter and having good reverse isolation, it is capable of the power output required for the mixer, which is not true of any of the other amplifiers. The Telonic filters shown were tunable bandpass filters with a 5% bandwidth which permitted noncritical tuning. The high pass filter indicated, which was made by the author, had a 70 MHz lower cut off.

According to the theory of the echo (Chapter 1, sec. 4), sufficient signal amplitudes on grid 2 will result in echo saturation. Considering the oscillator outputs indicated and the attenuation to the grids, one might suppose the amplitudes would be excessive, but the high capacitance of the grid support rings (300 Pf) results in almost complete reflection of the signals. It has been determined by use of the set-up to be next described, that the work has been done at amplitudes at which the echo amplitude is proportional to the grid 2 signal amplitude.

The arrangement for saturation of the echo is shown in Figure 6. Because the applied signal level was higher in this case, less reverse isolation was required. In this case, the high power oscillator was

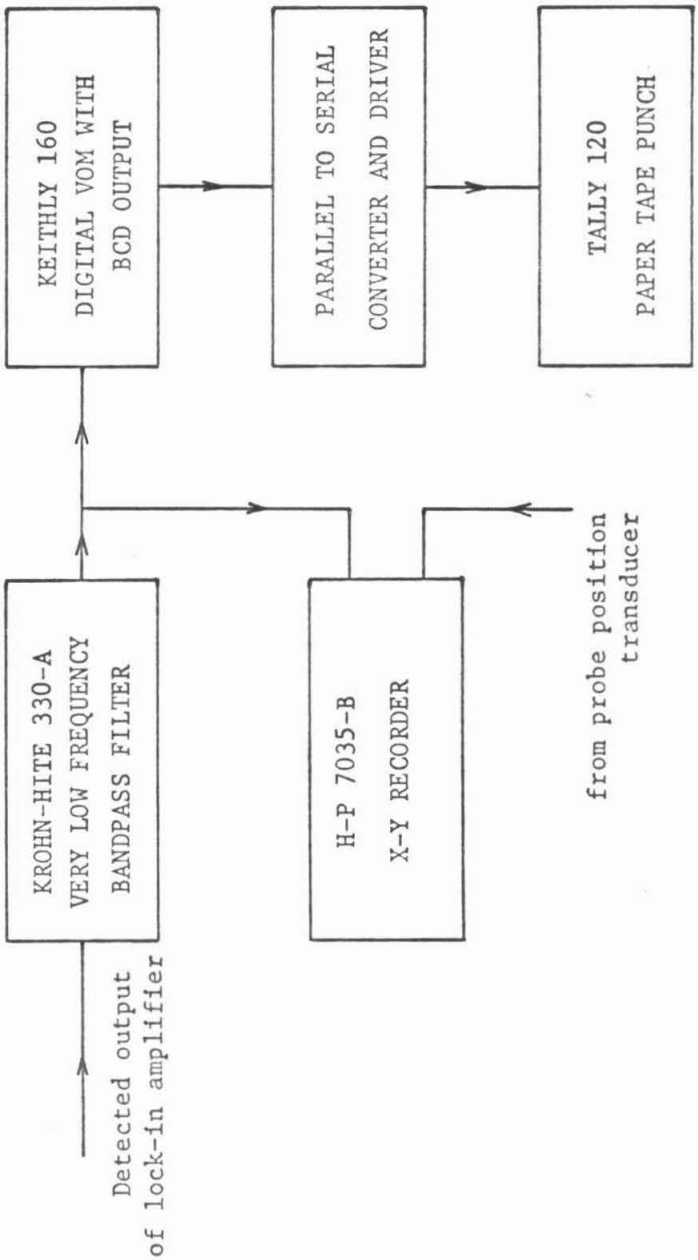

Fig. 7. Signal Processing

used in the grid 2 circuit, so that the amplitude could be varied over a large range. Using the two General Radio amplifiers (which do not oscillate together) in place of one of the Radiation Devices' amplifiers merely allowed the P.A.R. lock-in amplifier to be used in a less sensitive range.

2.5 Signal Processing

The unique part of this experiment is the signal processing system following the lock-in amplifier. The arrangement is shown in Figure 7.

The receiving probe is driven by a synchronous motor so that there is a fixed relation between echo wave number and the frequency of the lock-in amplifier output signal.

The output of the lock-in goes into an active very low frequency bandpass filter, the upper and lower cut-off frequencies of which are separately adjustable from .02 Hz to 2 KHz in five ranges. The upper cut-off is considerably sharper than that of the one pole filter in the lock-in, while the lower cut-off is used to remove unwanted long wavelength modes excited by the echo.

The filtered output is recorded on an X-Y recorder during the experiment to provide an immediate record of a run.

The same output is the input for three figure (plus an overflow bit) digital voltmeter with a B.C.D. output and a fixed sampling rate. The punch control, which was built by the author, converts the parallel output of the voltmeter into a series of BCD characters, as well as generating parity and zero bits and an end of word character after each word. It was also possible to set up an arbitrary character

and initiate a punch manually. The device took advantage of the great variety of integrated logic now available, as well as using discrete devices to drive the selector solenoids of the paper tape punch.

The bandwidth of the filtered signal is between .02 and .05 Hz, so that the one sample per 2 second rate is far more than enough to permit an alias free sample. Some early runs were done at higher speeds and proportionally higher sampling rates.

The purpose of digitizing the echo is to permit a Fourier transform of the signal to be done by a computer. The information on the paper tapes was first put on punched cards, which were more convenient for the following processing steps.

Because broad band noise in the echo bandwidth would be added to the value of the transform at that frequency, such noise would result in an erroneous measure of echo damping. Two techniques were tried to reduce this problem.

The first approach was to run the probe at a high speed (resulting in frequencies around .1 Hz) but take several such runs. The raw data were then arithmetically averaged into a single run. It was a technique which did help, but it was tedious because of the number of runs required to achieve a significant noise reduction.

Improvements were gradually made in the RF electronics to reduce the noise related to probe motion (plasma and receiver noise were never really a problem). This combined with reducing the probe speed to give a center frequency of about .03 Hz gave better results than averaging. Although the noise was mostly eliminated, a residue of the unwanted long

wavelength echo modes often remained. This was a problem because truncation of the time domain signal at a finite amplitude would contribute to all frequencies of the transform. To remedy this, a digital filter program was written by the author using an impulse invariant technique (Rader and Gold [33]). The filtered or averaged echo was then Fourier transformed using a fast Fourier subroutine supplied by the C.I.T. Computing Center. The method was based on that by Cooley and Tukey [34]. Because the phase of the transform had no meaning without knowing the phase of the echo, the magnitude of the transform was taken, which meant the square root of the power spectrum was found. The significance of this quantity to the echo is given in Chapter I.

An added benefit of digitizing the echo is being able to have computer plots of all experimental data, which eliminated much tedious or expensive drawing.

CHAPTER 3. EXPERIMENTAL RESULTS

3.1 Echo Saturation

In order to insure against echo saturation complicating interpretation of the damping experiments, it was necessary to find at what exciter amplitudes and separations saturation did occur. Not only were these conditions found, but better agreement with the theory (Section 1.4) was observed than in the work of Ref. 22, the only other saturation experiment known to the author.

No study of the echo saturation with frequency was attempted, both because the apparatus was limited in frequency range and because the main objective of the experiments was to measure diffusion in velocity space. The results to be described were done with $\omega_1/2\pi$ = 300 MHz, $\omega_2/2\pi$ = 550 MHz , and exciter separation ℓ = 7.9 cm.

As was shown in Section 1.4, the saturation of the echo depends strongly on the velocities of the electrons contributing to the echo. For the second order echo used in these experiments, the spread in contributing velocities is such that although there is a general saturation of the echo with increasing grid 2 amplitude, the J_1 Bessel function behavior predicted in Section 1.4 is not at all visible in the original data.

Figures 8a-8d show the echo amplitude in position space for various grid 2 relative amplitudes. Note the change in amplitude scale in the different figures. Only a relative exciting amplitude is indicated because the potential at the grids is far less than that at the generator because of the high grid support capacitance. In Section 3.2 a value of the grid potential will be estimated and compared with that deduced from the echo saturation.

As can be seen from Figure 8, only a small range of wave numbers contributes to the echo, so that the Fourier transform of the echo consists essentially of one peak. Because a wave number k corresponds to a velocity $v = \omega_3/k$ (Section 1.4), one can observe the saturation as a function of velocity for those velocities in the peak.

By plotting the magnitude of a Fourier component of wave number k from each run against the relative amplitude ϕ_2 applied in that run, one obtains the experimental points shown in Figs. 9a-9c. According to (22), Section 1.4, the points should correspond to $|aJ_1(b\phi_2)|$, where a and b are functions of k and applied frequencies, and a is proportional to ϕ_1, the grid 1 voltage. The most interesting feature of these curves is the approach to 0 of the echo amplitude as ϕ_2 increases. A perfect null is difficult to observe because the received RF leakage increases with ϕ_2 so that even if the echo were perfectly nulled, there would be some signal remaining.

a and b can be determined from a given curve by observing that as $\phi_2 \to 0$, $aJ_1(b\phi_2) \to ab\phi_2/2$, which is the slope of the curve at $\phi_2 = 0$, while $a/J_1(j'_{1,1})$ is the peak of the curve, where $j'_{1,1}$ is the first zero of J'_1. Using these a's and b's, the solid curves of Figures 9a-9c were computer drawn.

The actual J_1's have a shorter period in some cases than the experimental data, but one must recall that the J_1 dependence arose from a two term series expansion in the perturbed electron velocity which may not be perfectly valid at the higher amplitudes.

If one assumes the excitation suggested at the end of Section 1.4, b should have the velocity dependence $[1 - \cos(h\omega_2/v)]/v^2$ if the

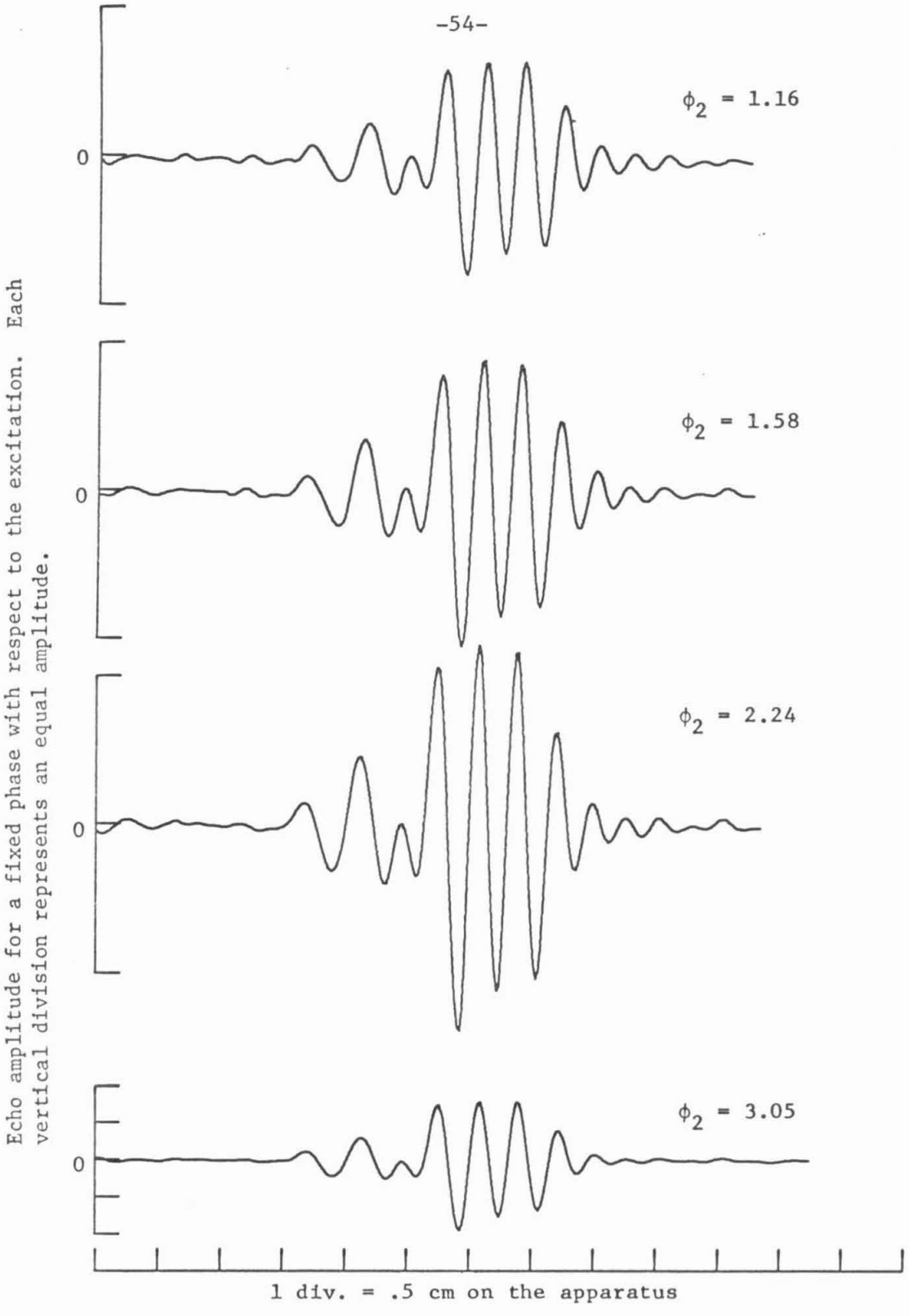

Fig. 8a: Saturating spatial echo for various grid #2 amplitudes ϕ_2

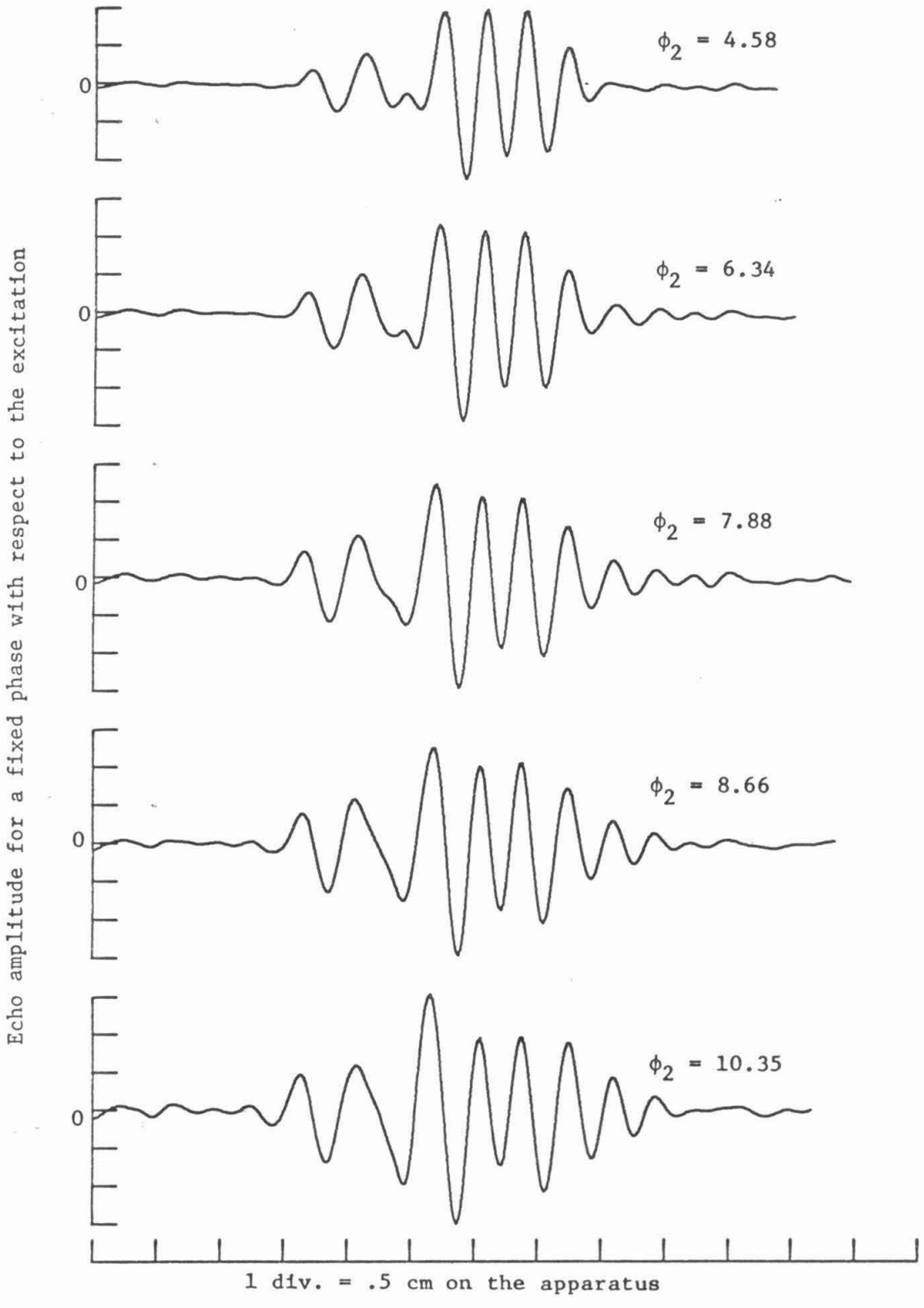

Fig. 8b. Saturating spatial echo for various grid #2 amplitudes ϕ_2

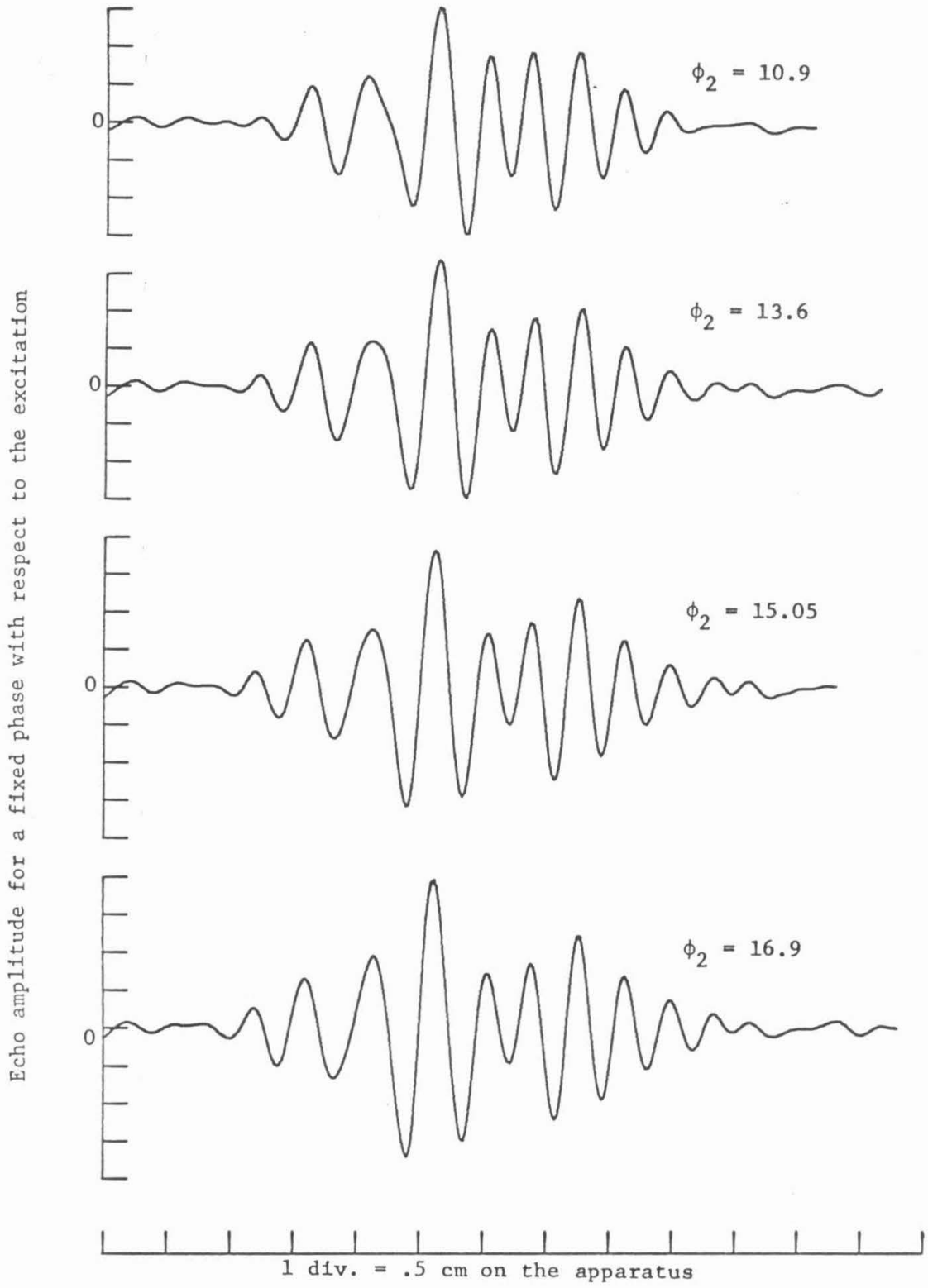

Fig. 8c. Saturating spatial echo for various grid #2 amplitudes ϕ_2

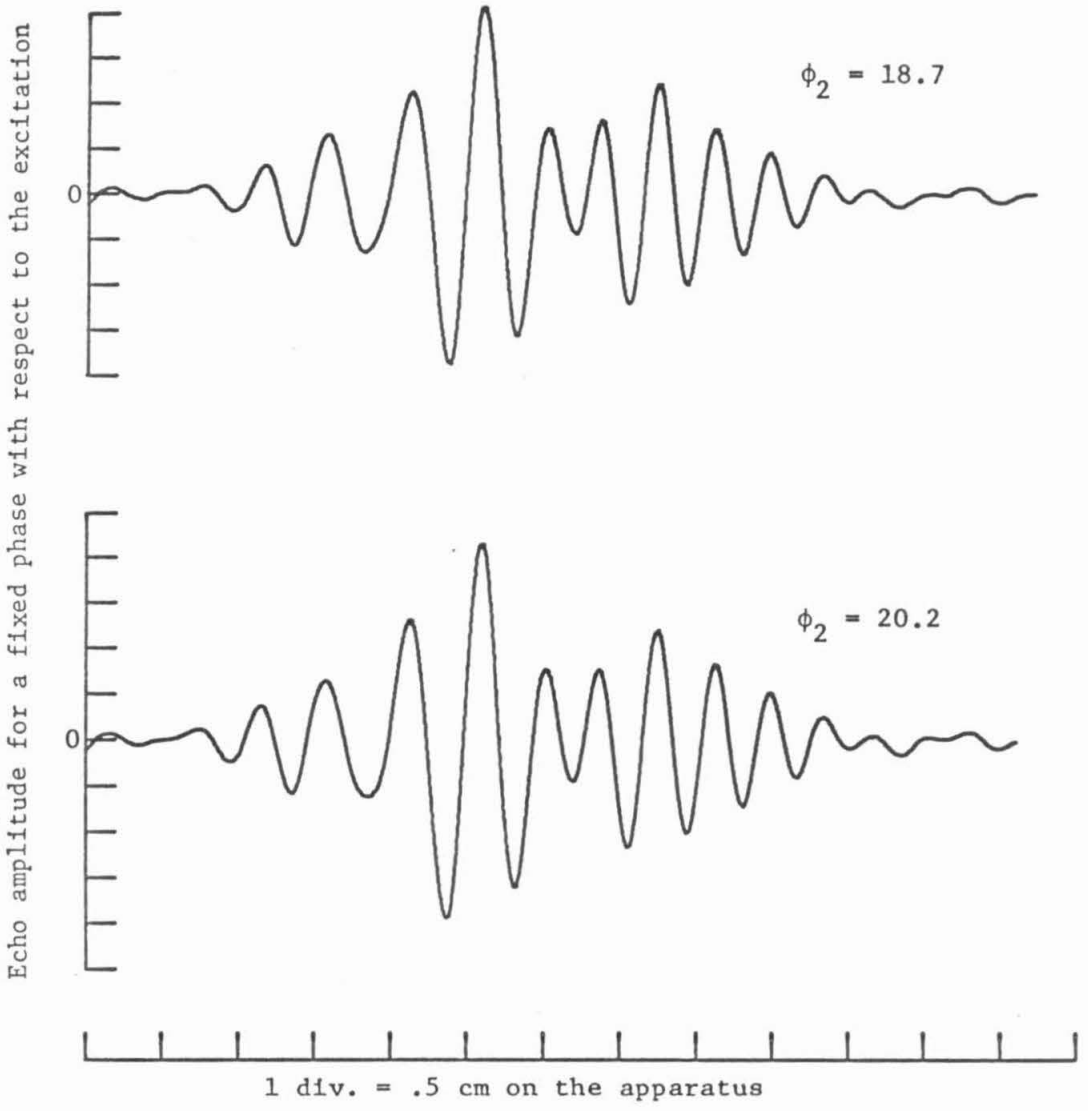

Fig. 8d. Saturating spatial echo for various grid #2 amplitudes ϕ_2

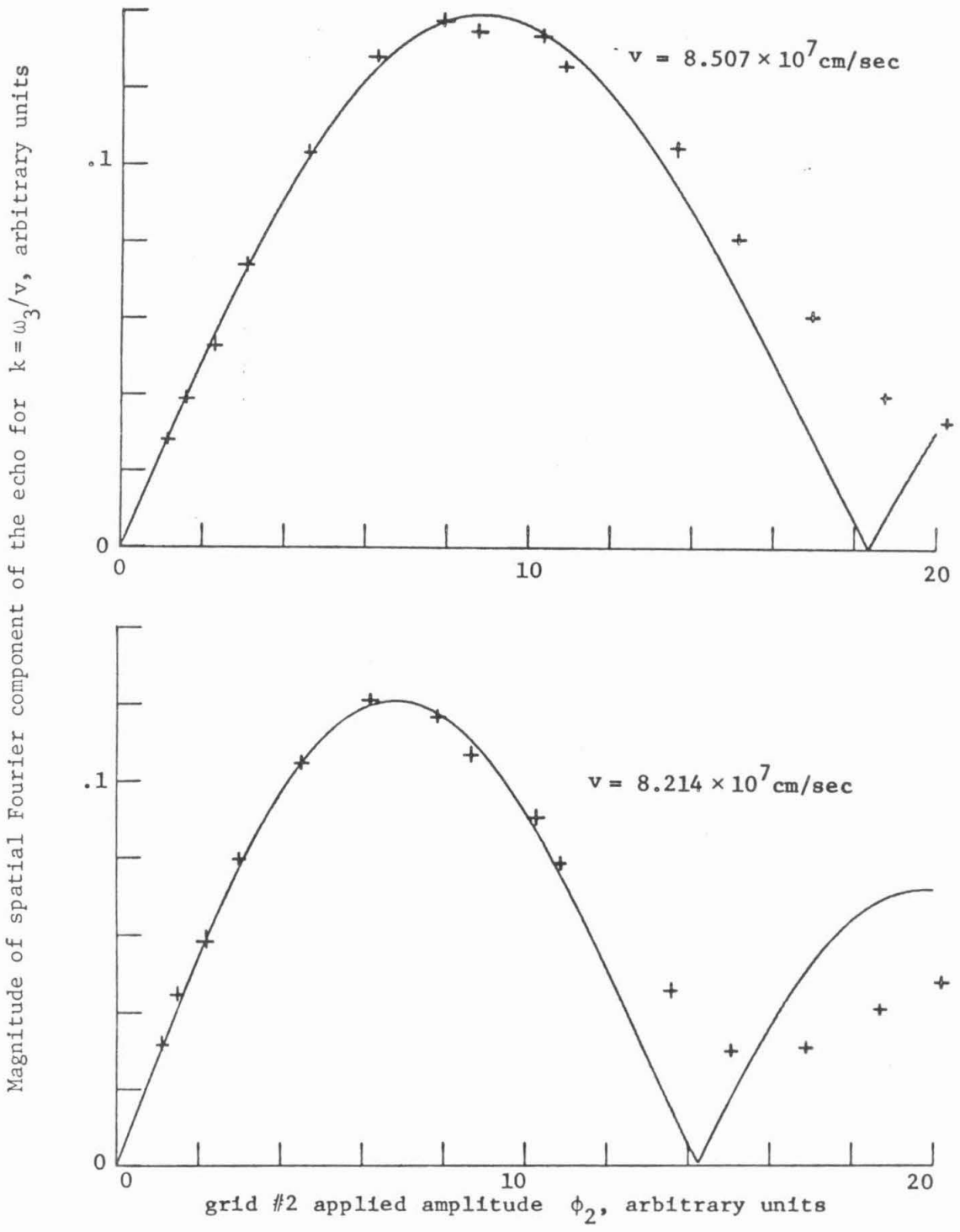

Fig. 9a. Echo saturation with $aJ_1(b\phi_2)$ fitted to experimental points

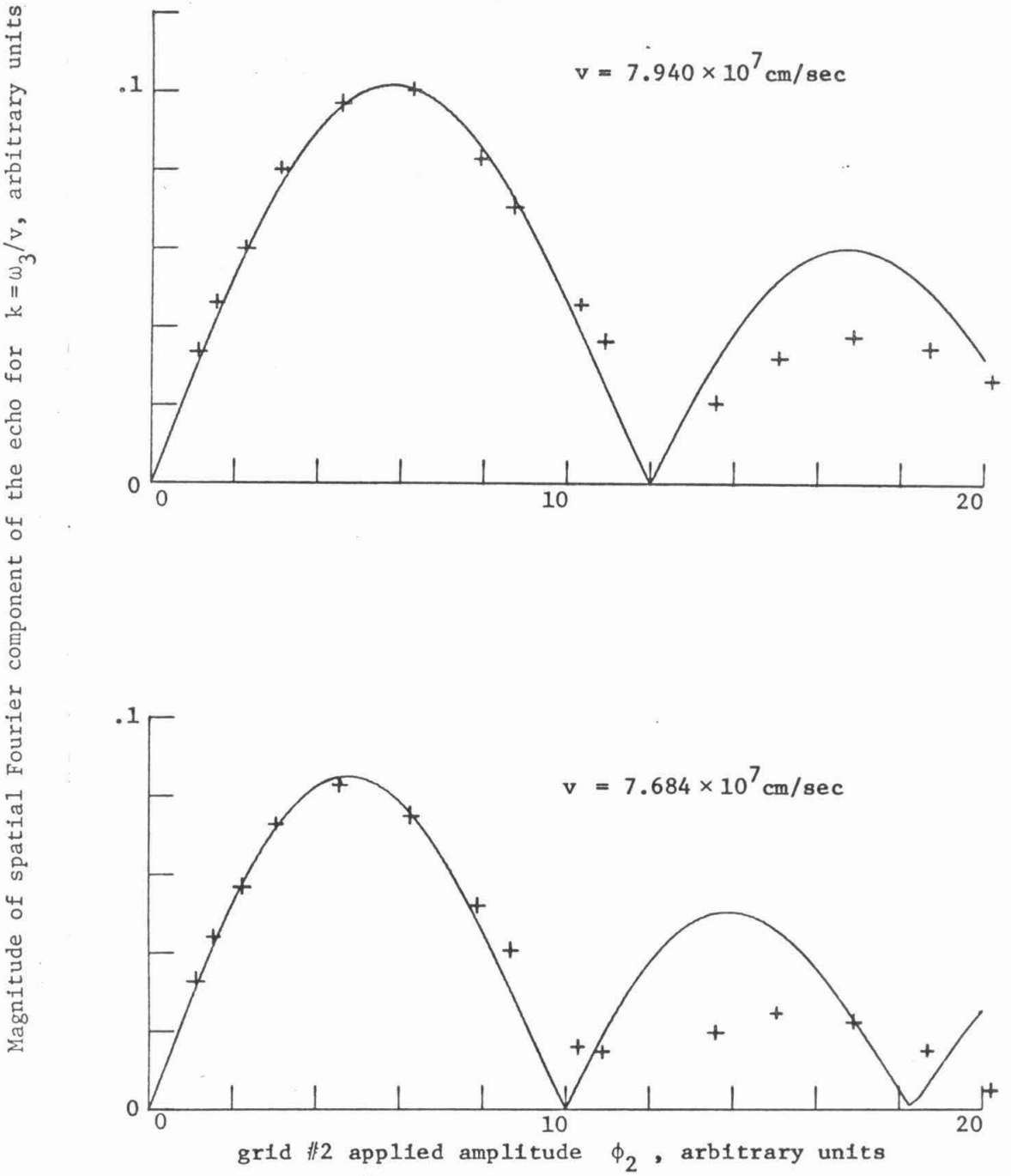

Fig. 9b. Echo saturation with $aJ_1(b\phi_2)$ fitted to experimental points

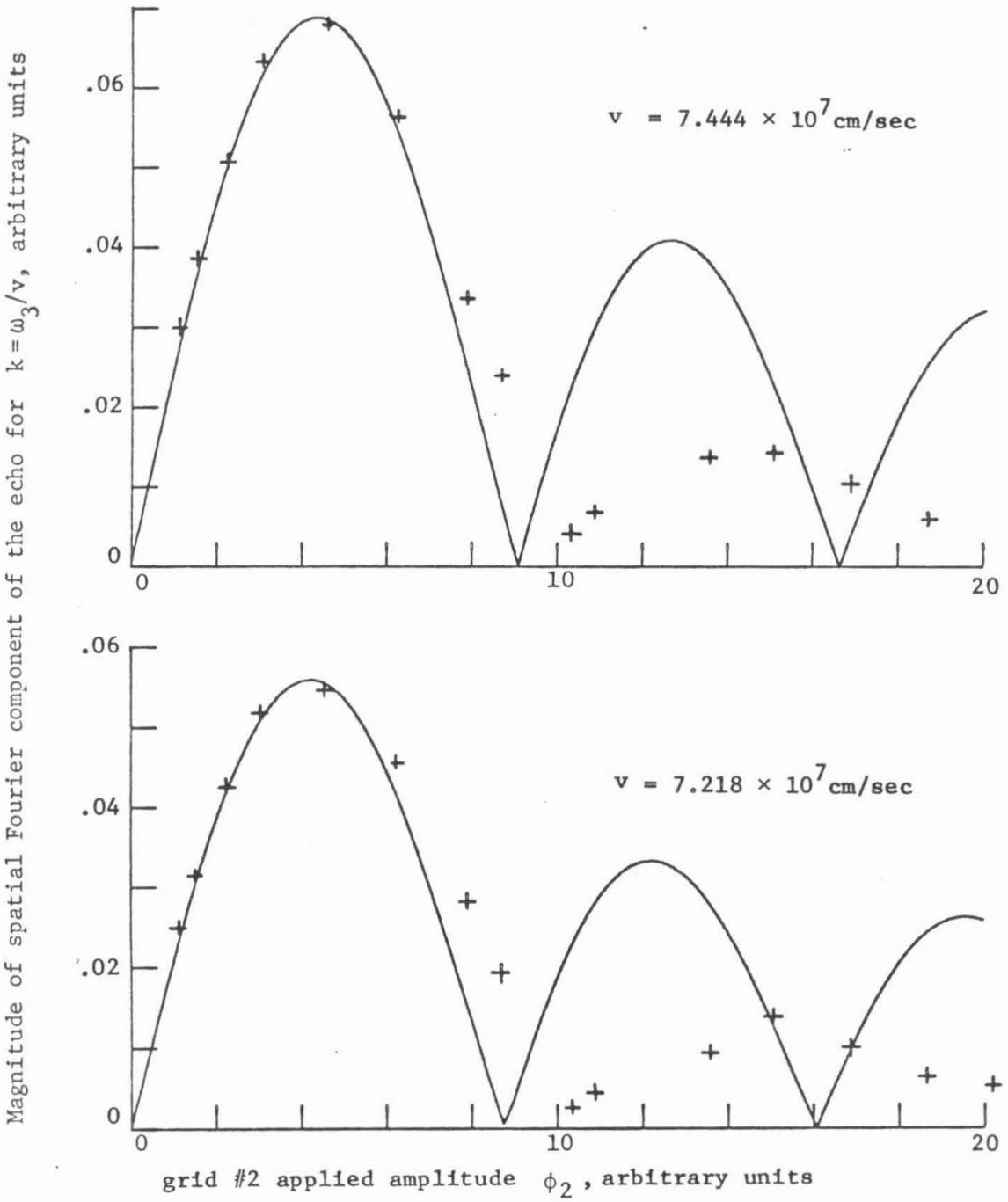

Fig. 9c. Echo saturation with $aJ_1(b\phi_2)$ fitted to experimental points

dielectric function is constant, where h is the effective grid separation. It is reasonable to assume the dielectric function is constant, because its frequency argument is 6 times the plasma frequency. By plotting bv^2 for the b's of Figure 9, one obtains the points in Figure 10. The solid curve is $\sin^2[h\omega_2/2v]$ with h adjusted to best fit the experimental points. In fact, the value of h so obtained, $2.01 \pm .005$ mm, equals the approximately 2 mm grid spacing (which was never measured very accurately). This distance represents about 4 Debye lengths, so that it is difficult to tell if sheath thickness influences the effective spacing.

One can estimate the actual electric field at the grids by assuming the above excitation in which case the argument of J_1 is $\mathcal{E}_2\omega_2\ell$ e 4 $\sin^2[h\omega_2/2v]$ $/(m\omega_2 v^2)$. Choosing the velocity at the peak of the $\sin^2$, $v = 7.4 \times 10^7$ cm/sec. The argument of J_1 must equal $j'_{1,1}$ at the peak of the corresponding curve. This gives $\mathcal{E}_2 = 32.8$ v/m which gives a .065 volt potential with a 2mm grid separation. That gives a conversion factor of .021 volt/relative amplitude unit. The incident power from the 50 Ω source at that peak is 9.3 mw. Assuming a 170 pf (measured at 1 KHz) parallel load, that gives a peak potential of .030 volts at 550 MHz. However, at 550 MHz, part of the capacitance may be tuned out by inductance of the grid structure.

There are two significant features of the above results. The grid 2 amplitudes used in the damping work were about half the smallest value used in the saturation measurement, so that the echo amplitude is clearly proportional to the grid 2 amplitude and to ℓ in those measurements. More important is the verification that the Fourier transform

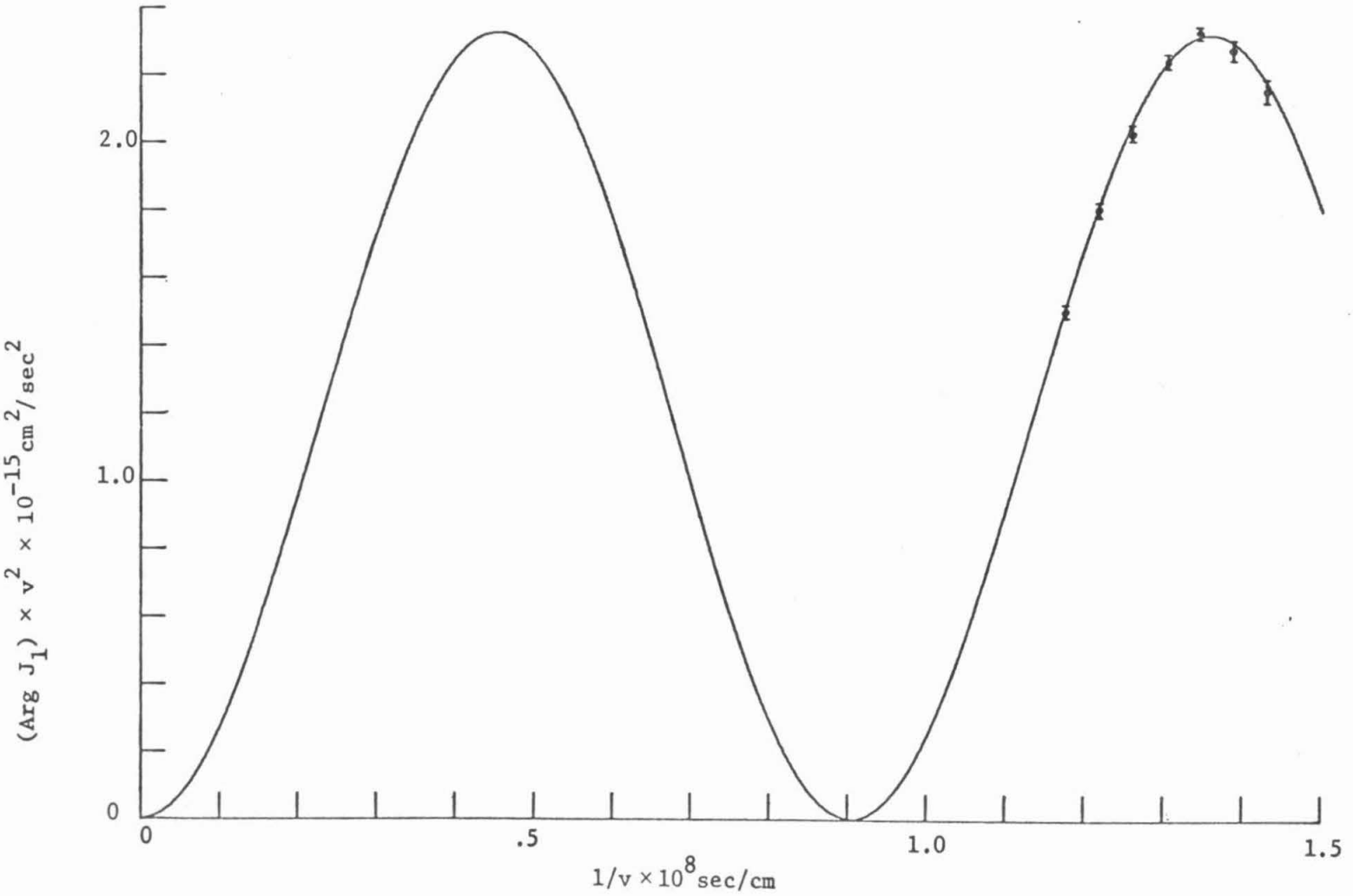

Fig. 10. $v^2 \times$ argument of J_1 as a function of $1/v$ (wave number of the echo)

really does separate velocity contributions to the echo, for any mixing of velocity contributions would make even this fair a fit to $|J_1|$ impossible.

3.2 Echo Damping Due to Coulomb Collisions

The main object of this work was to observe diffusion in velocity space as a function of velocity. In practice, the diffusion coefficient could only be measured over a limited range of velocity because the excitation of the echo was effective over a limited range of wave numbers. Further, over the small frequency range in which the receiver worked well, the wave numbers change with frequency to keep the range of phase velocities nearly constant.

For that reason, the data from the various exciter frequencies used all look similar. Therefore only the results at one pair of frequencies, $\omega_1/2\pi = 350$ MHz and $\omega_2/2\pi = 600$ MHz, are shown in what follows.

Shown in Figs. 11a-11c is the position space echo for various exciter separations. It is evident that although the overall amplitude is declining with increasing ℓ, the high wave numbers are disappearing more rapidly than the low wave numbers.

This effect is also evident in Fig. 12a, which shows the magnitude of the spatial Fourier transform of the echo as a function of wave number for various exciter separations, by a shift of the peak to the left. This figure also indicates which wave numbers, and therefore velocities, will give the most accurate indication of the dependence of damping on distance. The three tick marks (k_1, k_2, k_3) correspond to velocities 9.93×10^7, 8.21×10^7, and 7.22×10^7 cm/sec, respectively.

The shape of this figure for zero damping is predicted from (20) if some assumptions are made about f^o, the exciting electric field, and $\varepsilon(\omega_3, k)$. The exciting fields can be assumed of the same type as for Figure 10, in which case there is a single parameter h, the grid

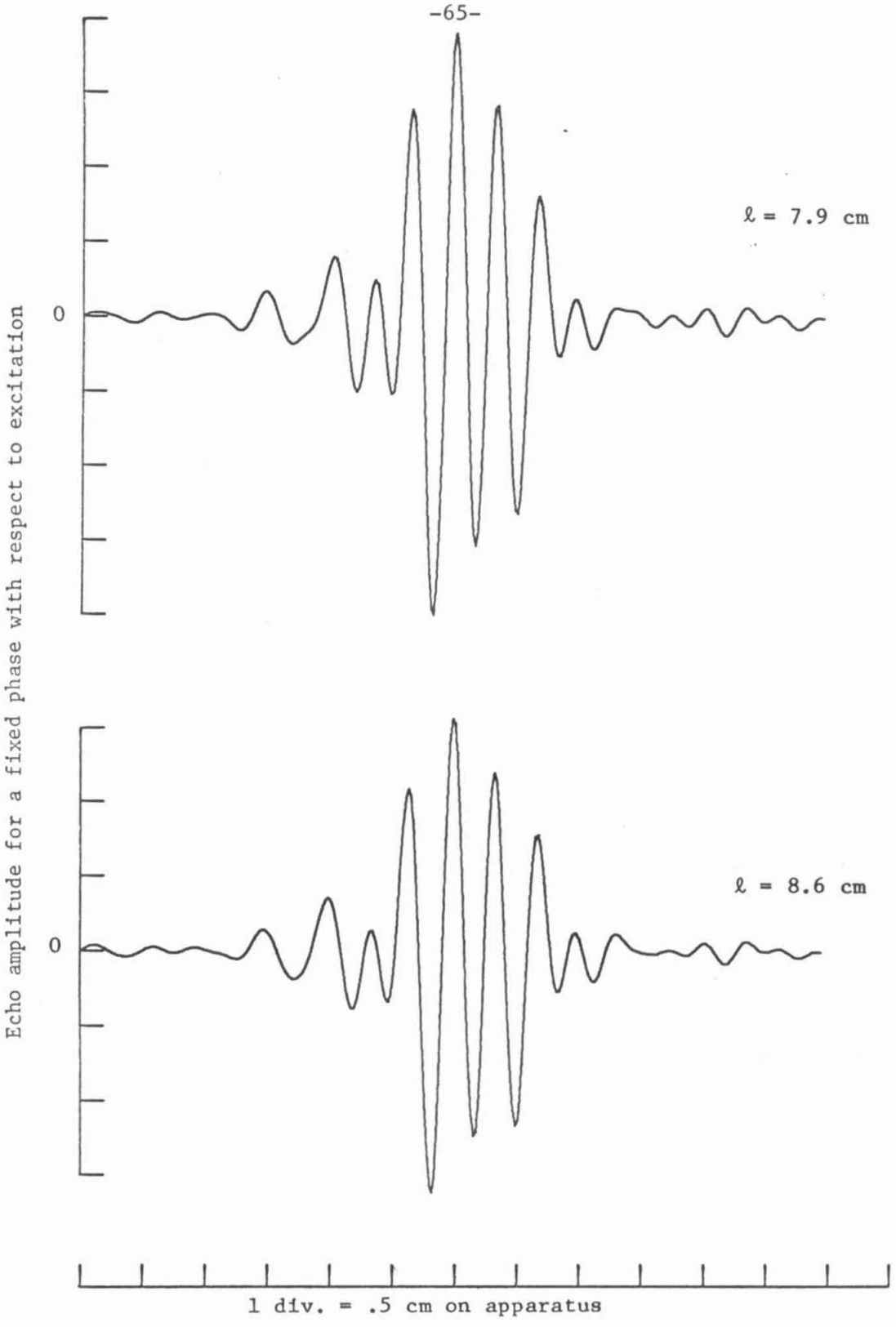

Fig. 11a Damped spatial echo for various exciter separations ℓ

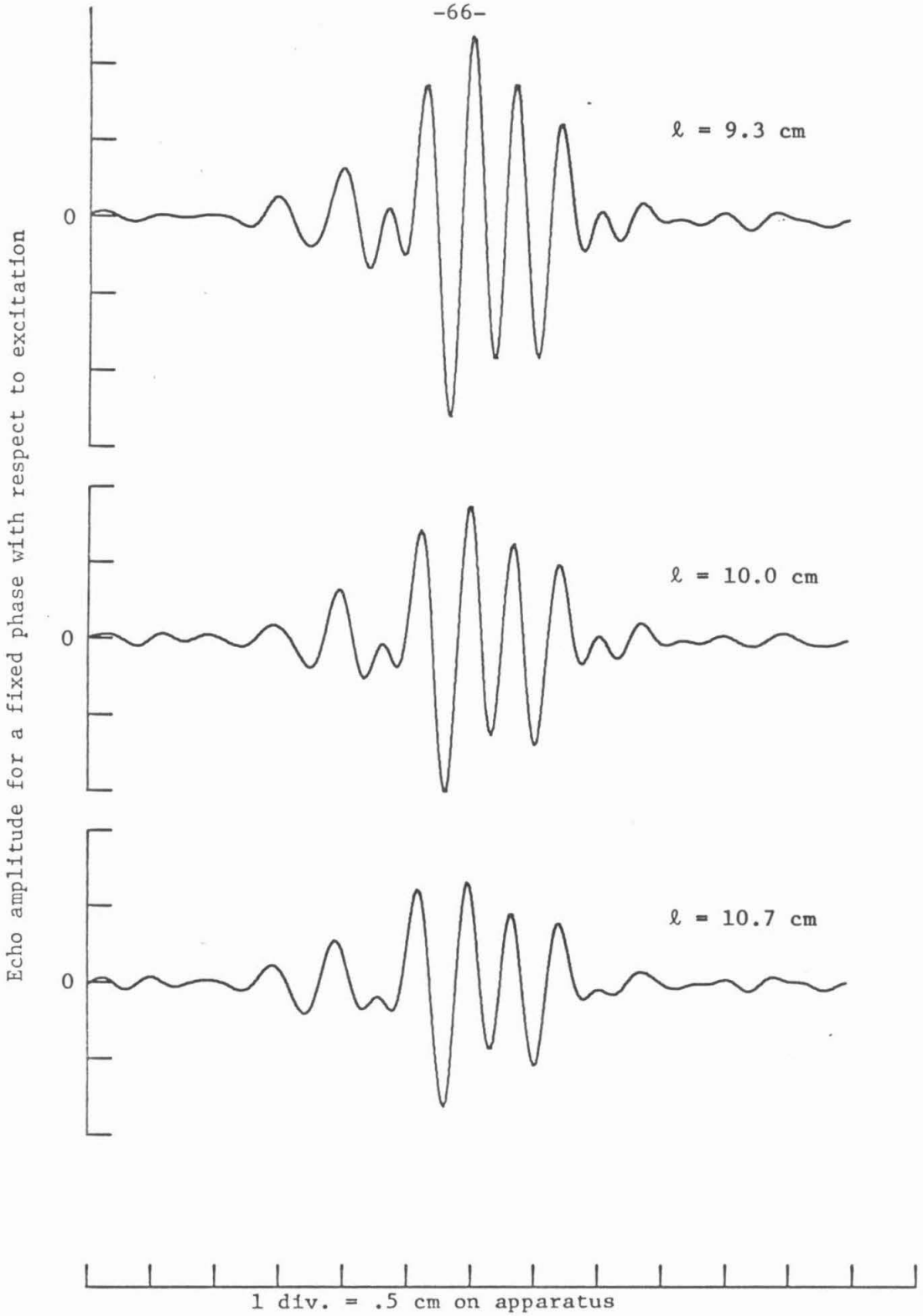

Fig. 11b Damped spatial echo for various exciter separations ℓ

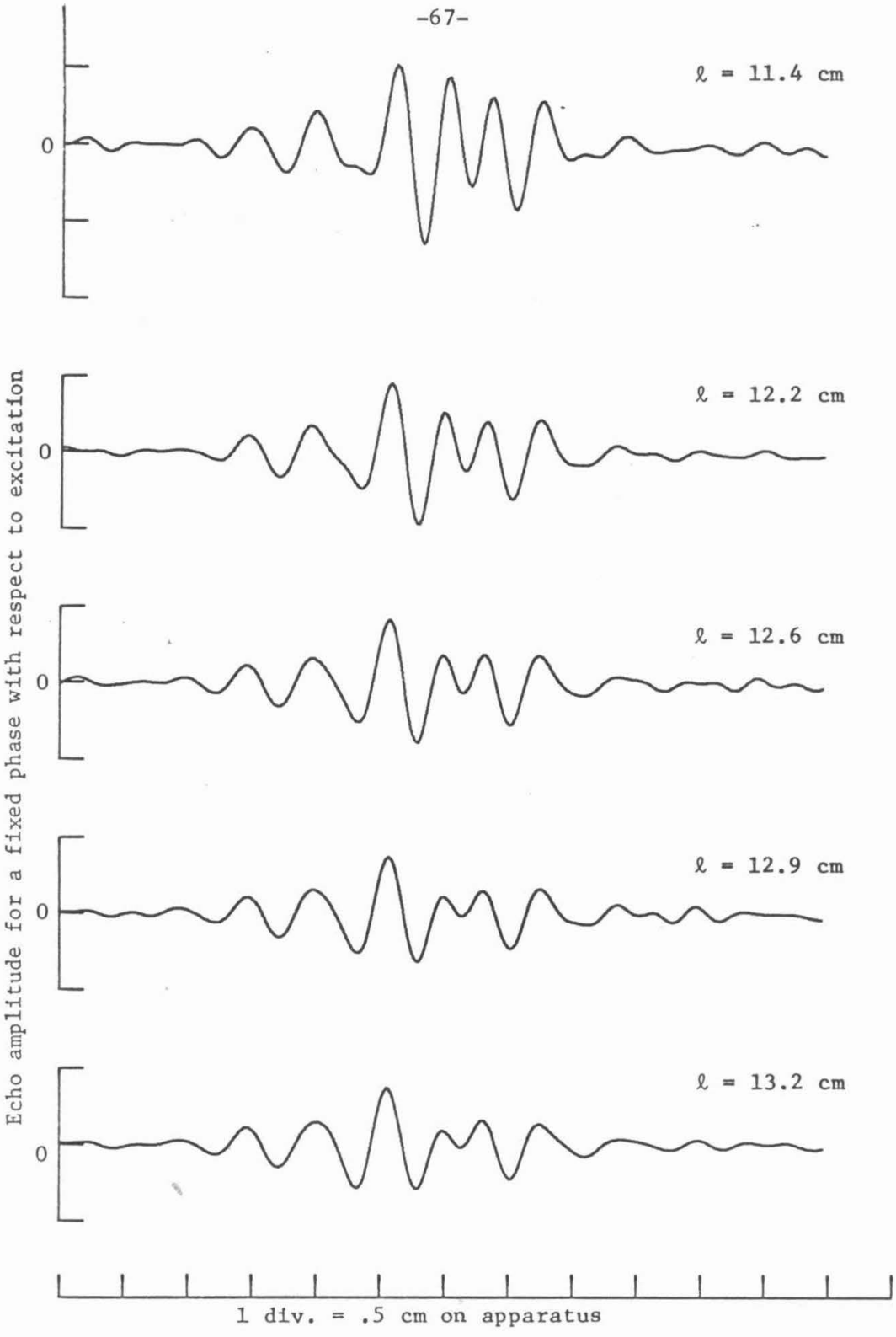

Fig. 11c Damped spatial echo for various exciter separations ℓ

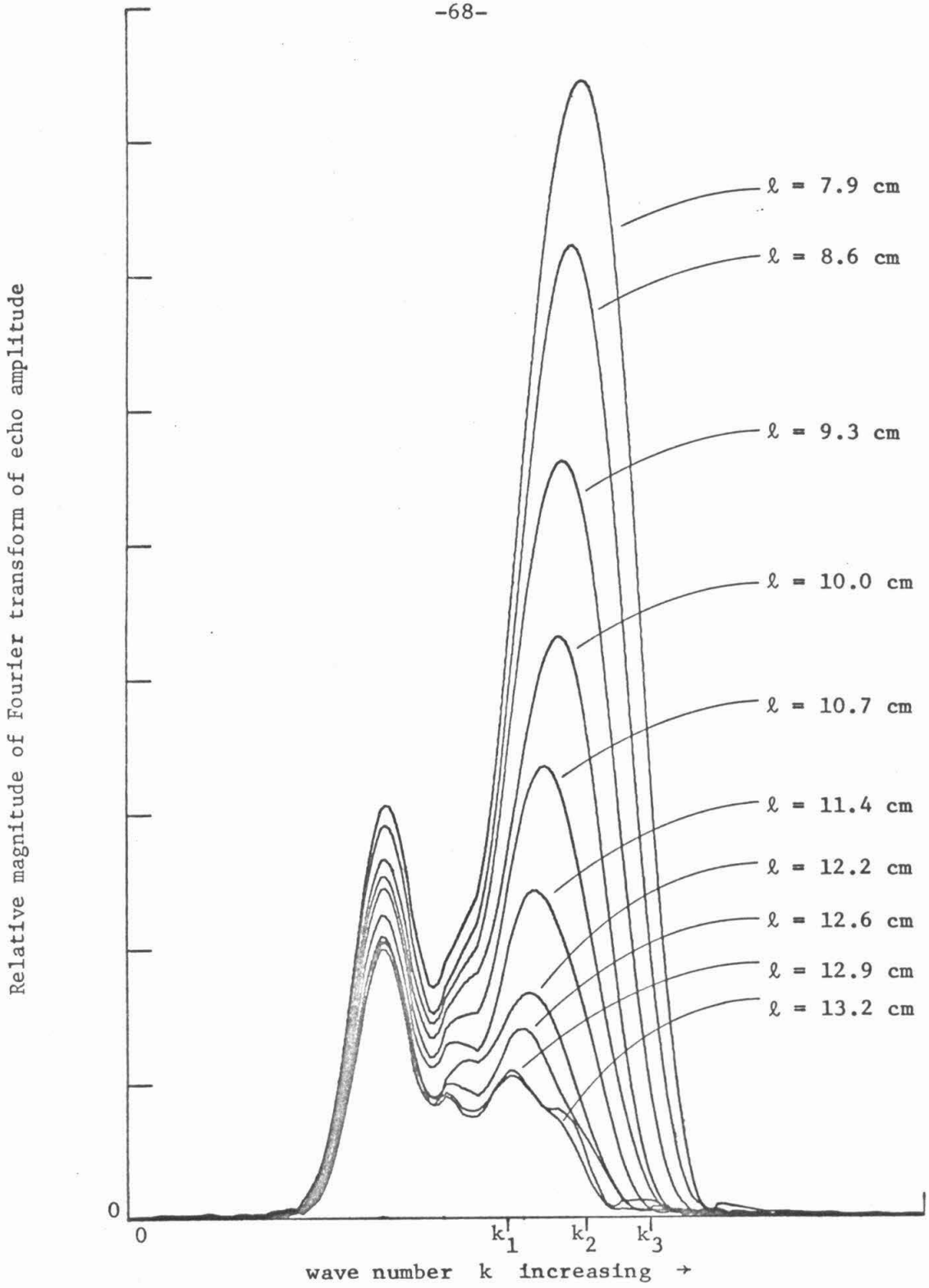

Fig. 12a. Fourier transform of echo as a function of k for various exciter separations ℓ

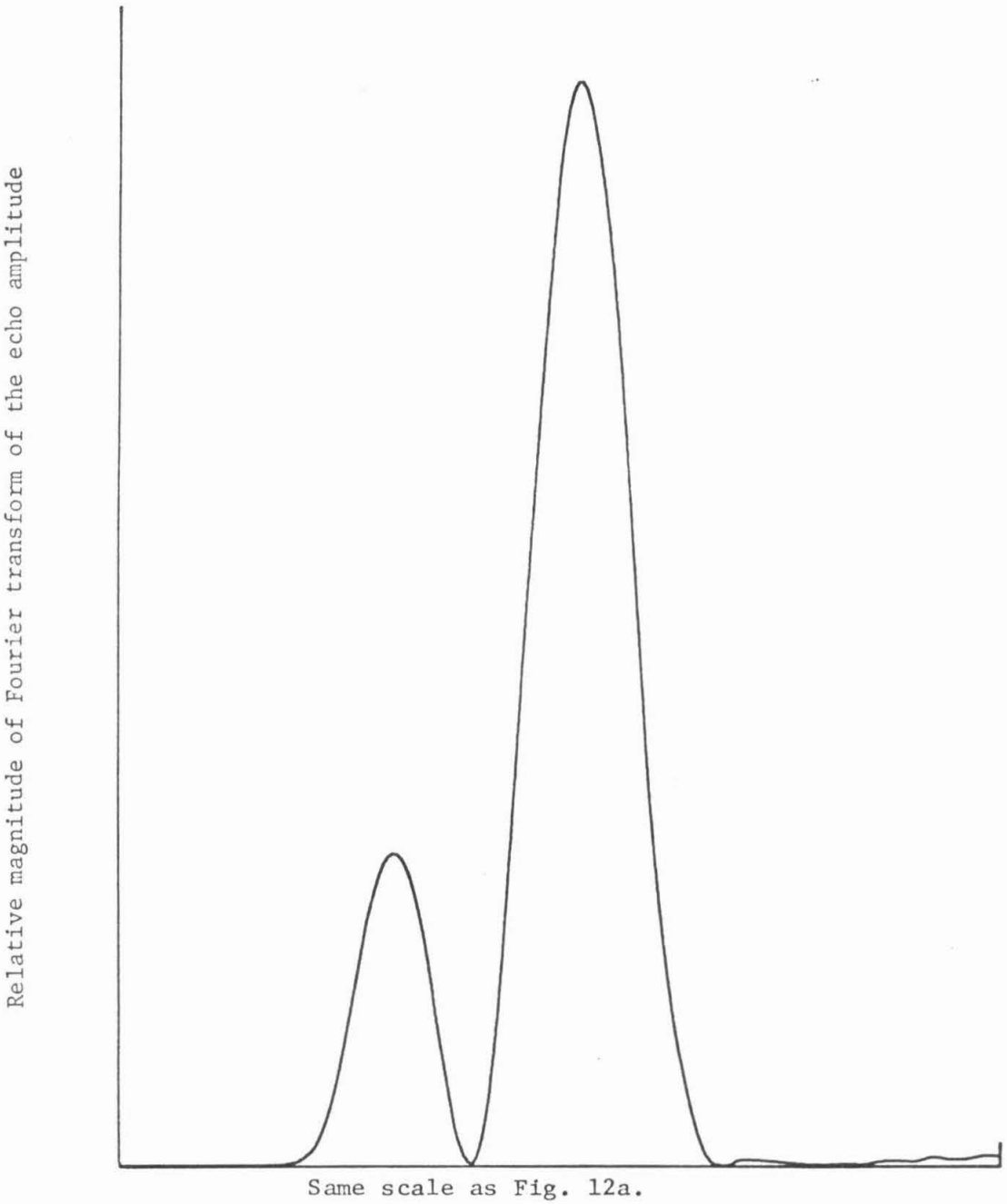

Fig. 12b. Fourier transformed echo as a function of k in the absence of damping predicted from equation 20a, Chap. 1

separation. With f^o taken as a Maxwellian, one can obtain a curve such as that of Figure 12b, with $n = 2.0$ mm (see Sec. 3.1) and electron temperature $t = 3$ eV. The effects of experimental filtering have been included in this curve.

Even with this somewhat unjustified temperature the position of the small peak and its relative height with respect to the larger peak are not correct. The position and height of the small peak is critically dependent on $\partial f_o/\partial v$, however, and for an f^o that has a larger high energy tail than a Maxwellian, the small peak would be higher and to the left. The effect of lowering the temperature is to suppress the lower peak, but not to significantly shift peak positions. As was shown in Section 2.3, a high energy tail with a temperature of even 3 eV is not inconsistent with the ion wave measured temperature of .62 eV.

Thus, the features of Figure 12a appear to be explainable by using a simple exciter model and a non-Maxwellian distribution, so that one need not assume $\varepsilon(\omega,k) \neq 1$ at the exciters. From the theory of Sec. 1.3, a Fourier component of the echo of wave number k results from the contributions to the echo of electrons of velocity $v = \omega_3/k$. Therefore, the data shown in Fig. 12a give, for a wave number k, the damping as a function of exciter separation ℓ for the velocity $v = \omega_3/k$.

From Sec. 1.3, equations (18) and (20), this Fourier component, in the absence of electron neutral collisions, should have the dependence $\ell \exp[-b\ell^3]$, where b is a function of wave number k. In the presence of electron neutral collisions, as was discussed at the end of Sec. 1.5, this dependence becomes $\ell \exp[-b\ell^3 - \ell'/\lambda]$, where

ℓ' is the total distance from the first exciter to the echo, and λ is the total mean free path for collisions between electrons of velocity v and the neutrals. $\lambda(v)$ has been determined experimentally (Brode [26]) for numerous gases.

There are various ways one could use this experimental data. The measurement of b was the main objective of this experiment, but beyond that, one could attempt to verify the cubic ℓ dependence, or determine $\lambda(v)$. There was not enough precision to determine all these quantities, however. It was decided to use the known value of $\lambda(v)$ for argon to correct the data for electron-neutral collisions, and then verify the cubic ℓ behavior and find b(v).

For a given wave number k , each data point was multiplied by $\exp[\ell'/\lambda(\omega_3/k)]/\ell$. For a wave number k_2 in Figure 12a, Figure 12c shows the effect of this correction on the data.

A $b\ell^3$ curve has been fitted to the corrected data. It is evident that for the smallest exciter separation, electron-neutral collisions dominate, while for the largest exciter separations, the diffusion damping clearly dominates.

In Figures 13a-13e, this corrected data for the indicated velocities has been plotted against $(\ell/\ell_o)^2$, $(\ell/\ell_o)^3$, and $(\ell/\ell_o)^4/2 + 3/2$, where ℓ_o is the smallest ℓ value used. k_3 and k_1 of Figure 12a correspond to the first and last values of velocity. The least scatter is in the area around k_2 . Although such a plot is not sensitive to the exponential, there is a definite curvature to the $(\ell/\ell_o)^2$ and $(\ell/\ell_o)^4$ plots which is absent in the $(\ell/\ell_o)^3$ plot.

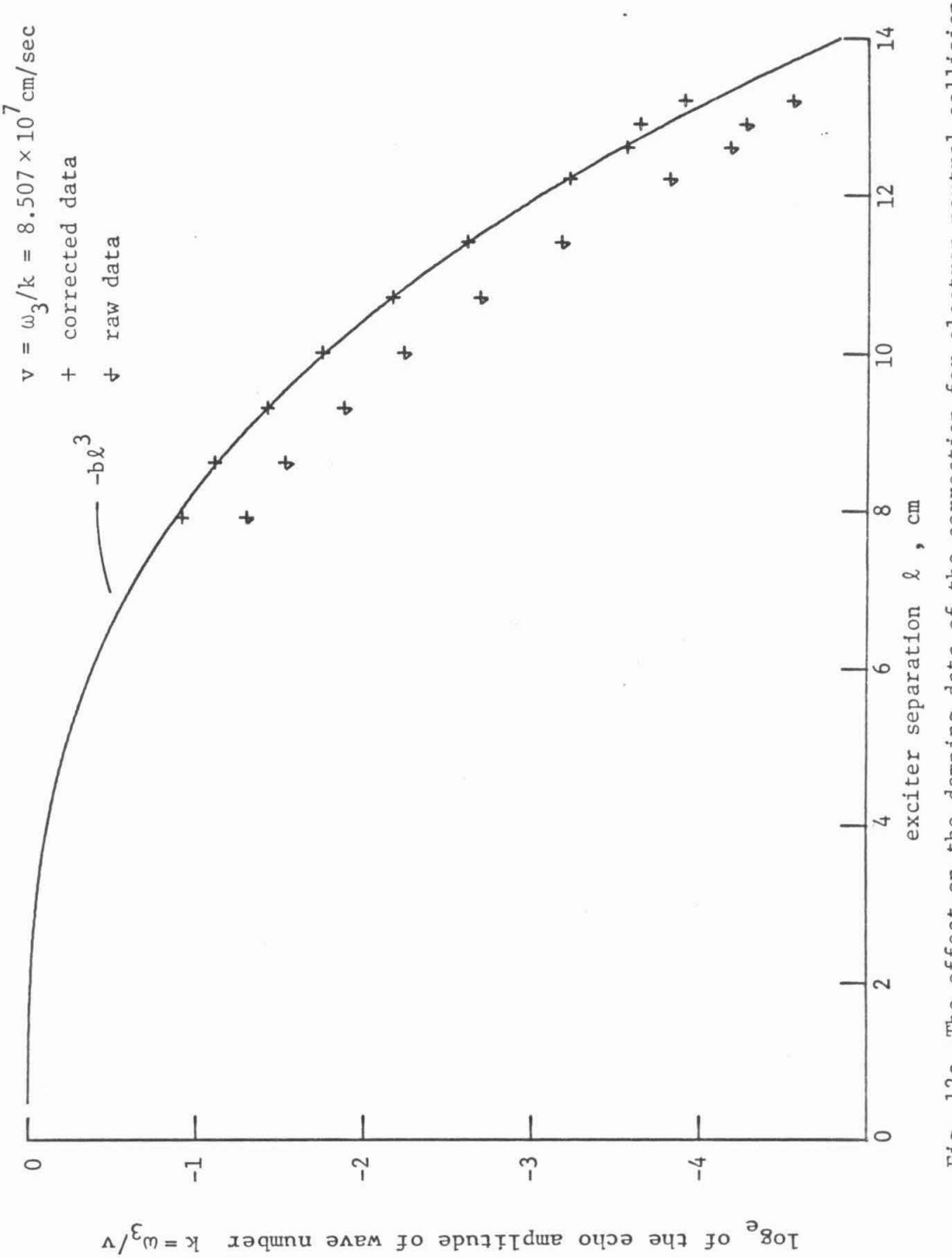

Fig. 12c The effect on the damping data of the correction for electron neutral collisions

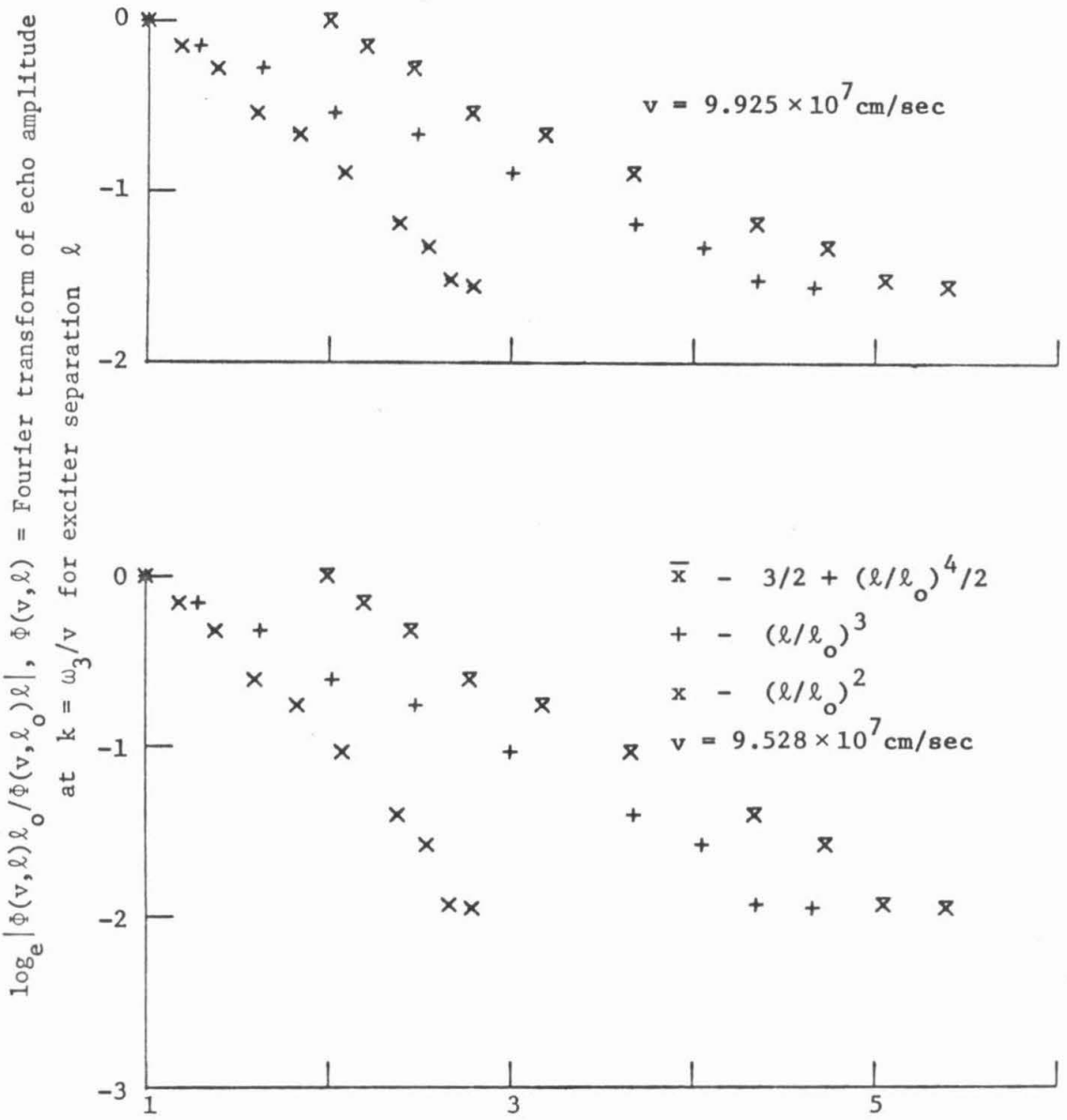

Fig. 13a. Echo amplitude plotted against various powers of exciter separation

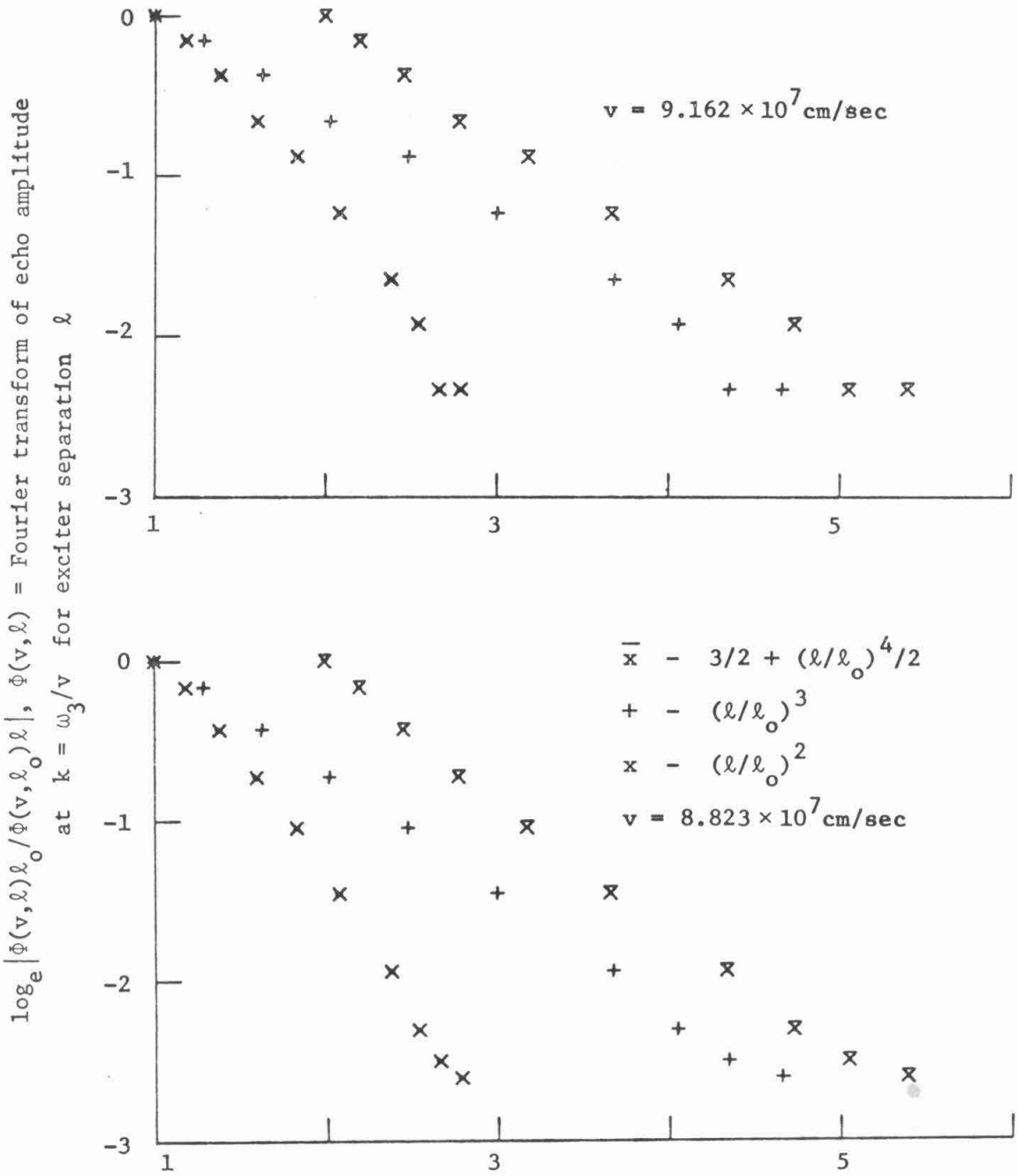

Fig. 13b. Echo amplitude plotted against various powers of exciter separation

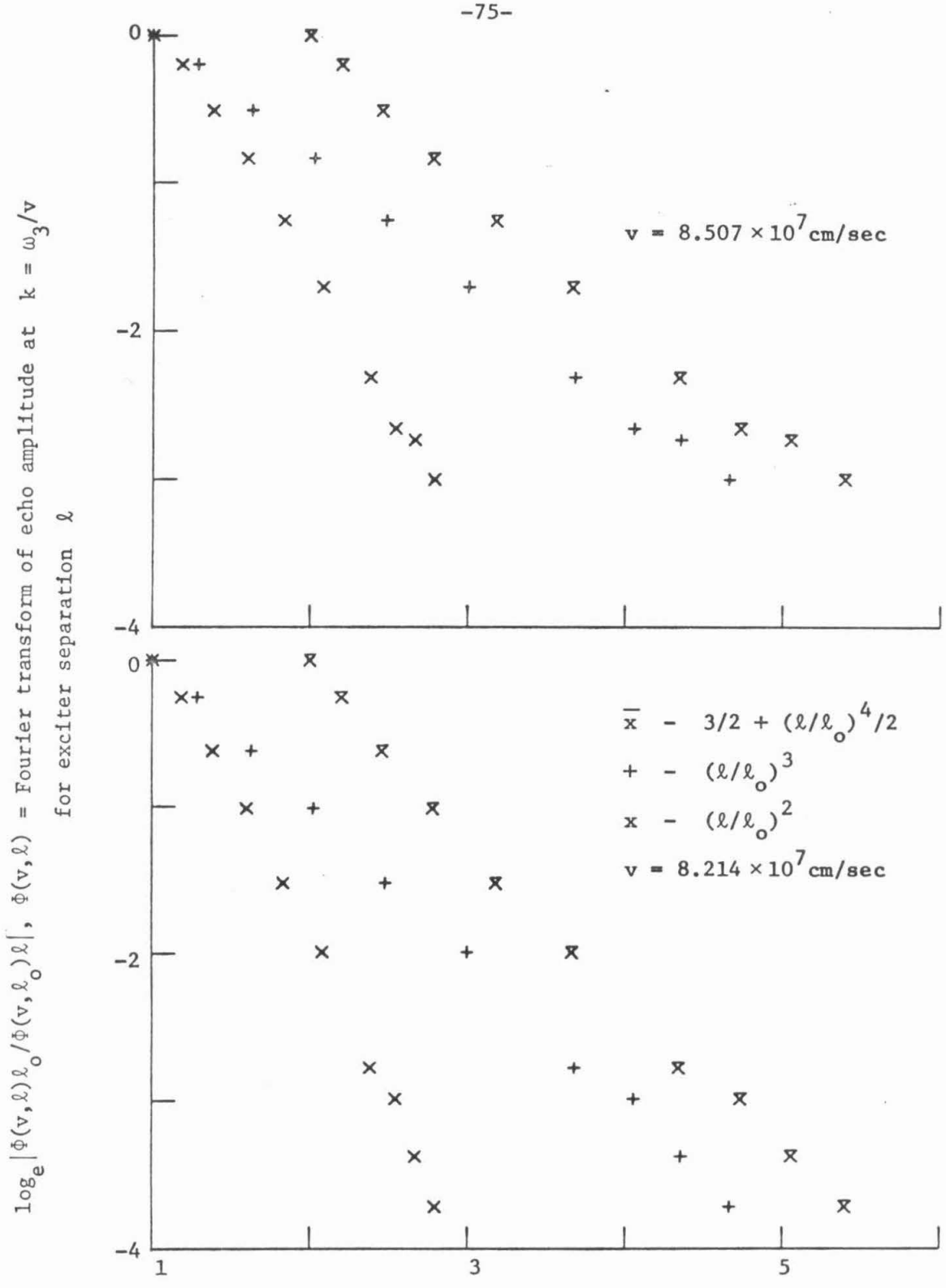

Fig. 13c. Echo amplitude plotted against various powers of exciter separation

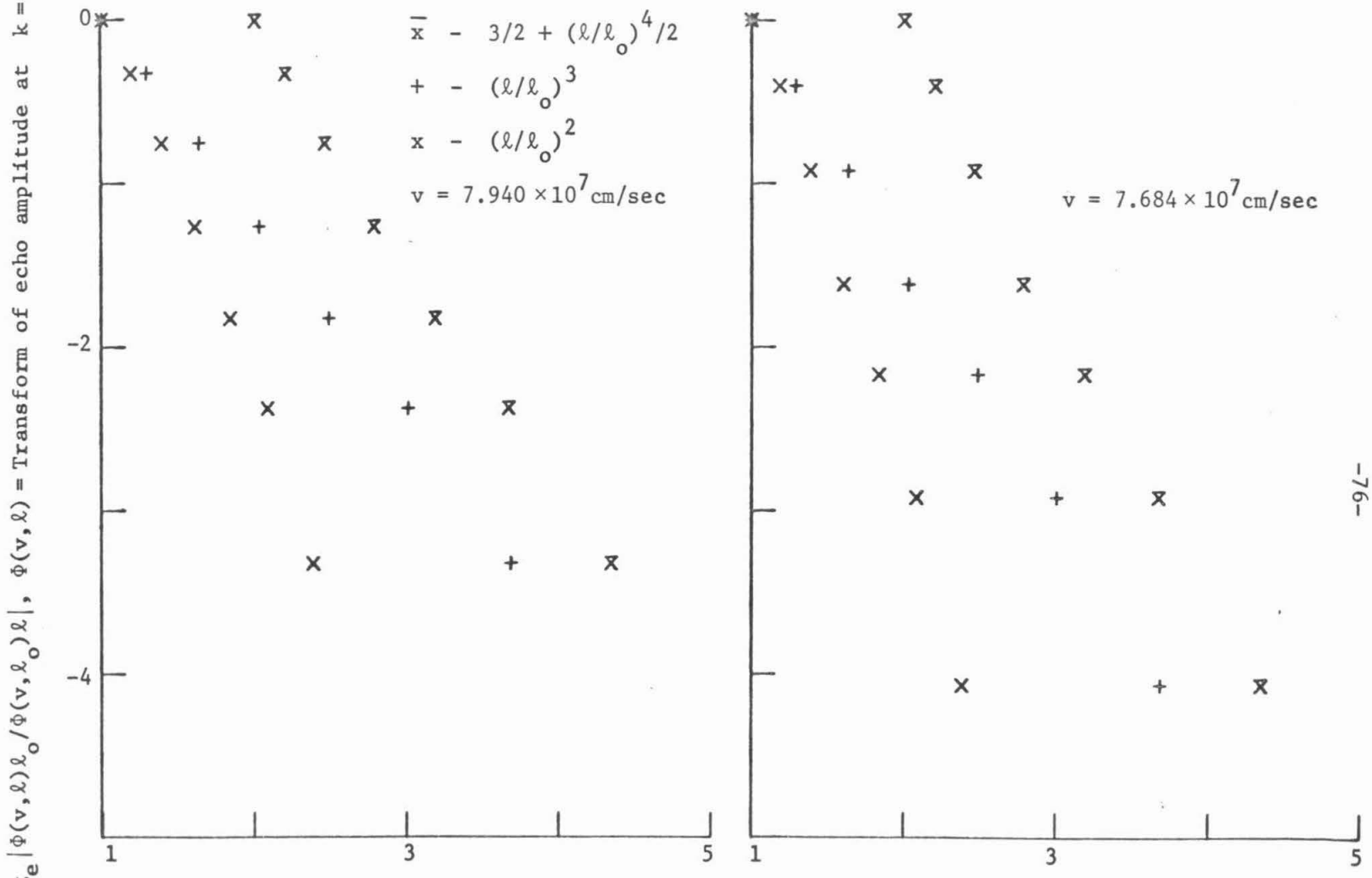

Fig. 13d. Echo amplitude plotted against various powers of exciter separation

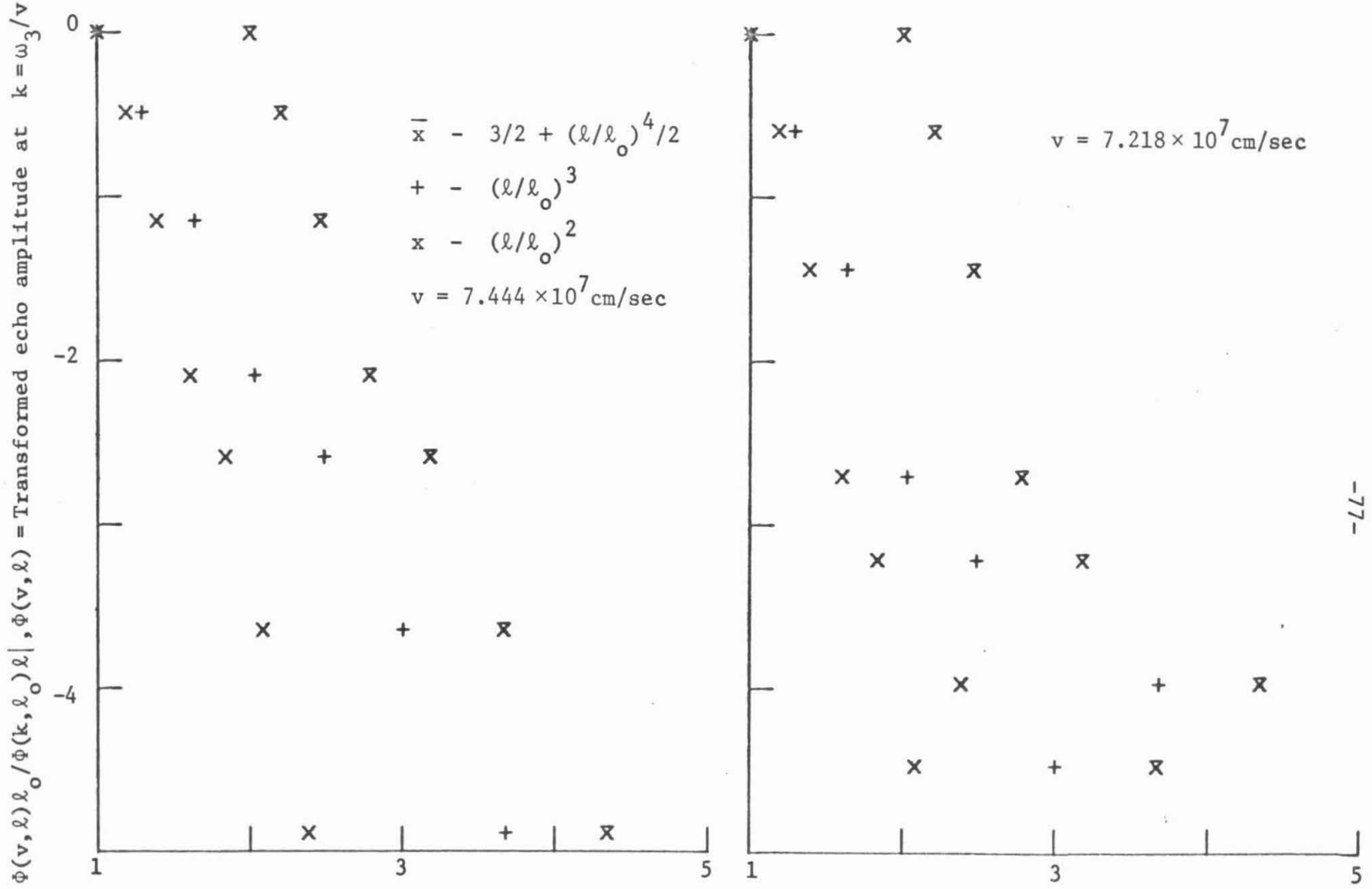

Fig. 13e. Echo amplitude plotted against various powers of exciter separation

While in principle one could improve the sensitivity by making a large number of runs, because of the 20 minutes required per run, the effect of plasma parameter drift could produce a systematic error over many runs.

The slopes of the ℓ^3 plots of Figure 13 can be used to plot the quantity b, the damping coefficient, in a $\exp[-b\ell^3]$ as a function of velocity. These values of b are shown in Figures 14a and 14b along with two sets of theoretical curves.

In Figure 14a, the diffusion coefficient D_{33} for a Maxwellian plasma in an infinite static magnetic field was used to evaluate the damping from equation (20b), Section 1.3, to produce the solid curves for the indicated temperatures. The plasma frequency used in the diffusion coefficient is the experimentally observed value

Although the observed damping falls within the curves, the velocity dependence is clearly weaker than predicted. Both a non-Maxwellian plasma and the actual finite magnetic field could qualitatively account for the discrepancy.

The diffusion coefficient is directly proportional to $\partial f_o/\partial v$, so that a non-Maxwellian high-energy tail in the electron velocity distribution would result in a weaker velocity dependence. Again, as was noted in Section 2.3, the ion acoustic waves that give a .62 eV electron temperature are not sensitive to high energy tails of even 3 eV, so that a non-Maxwellian plasma could easily account for the discrepancy.

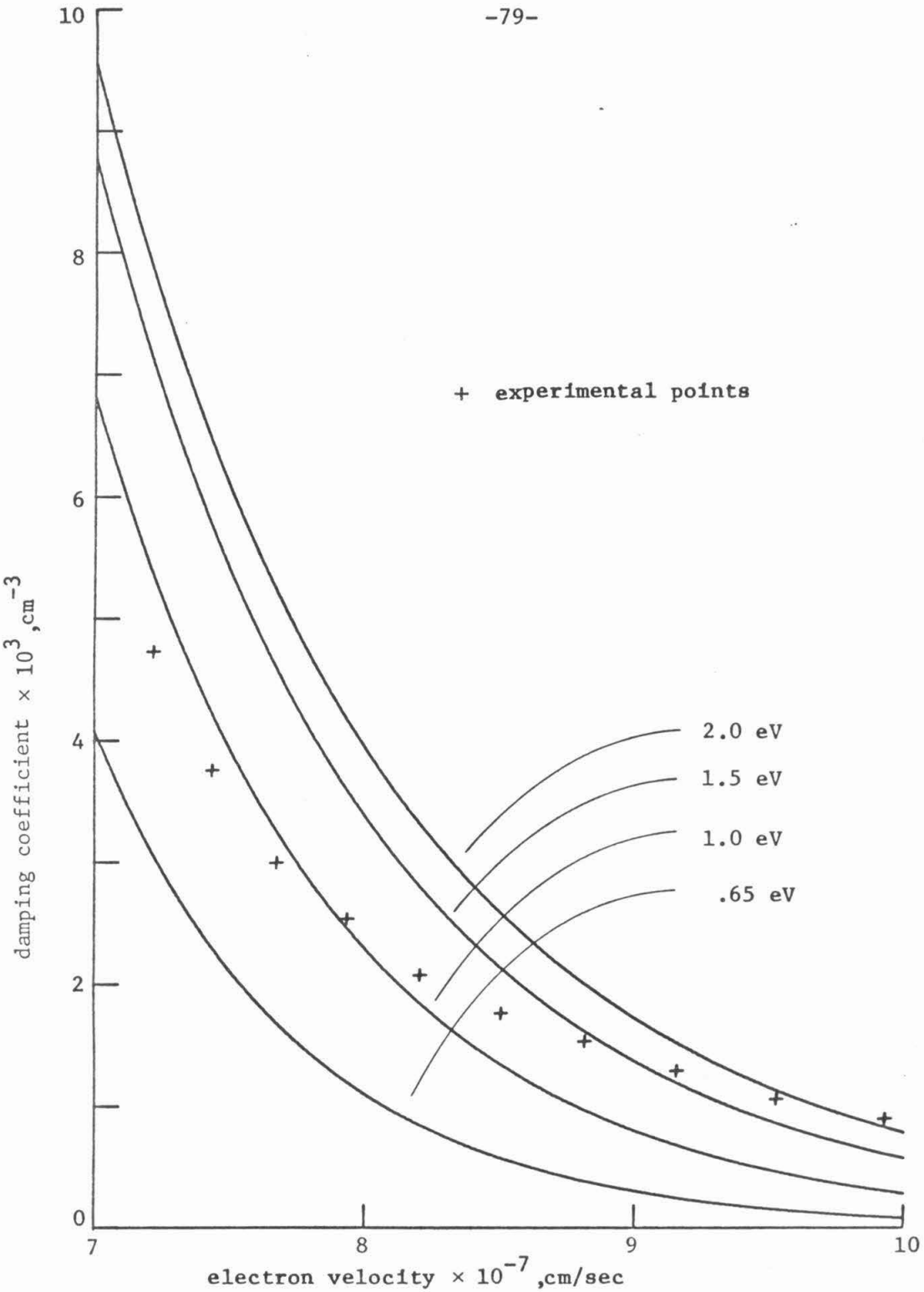

Fig. 14a. Damping exponent predicted from D_{33} for a plasma with infinite B_o .

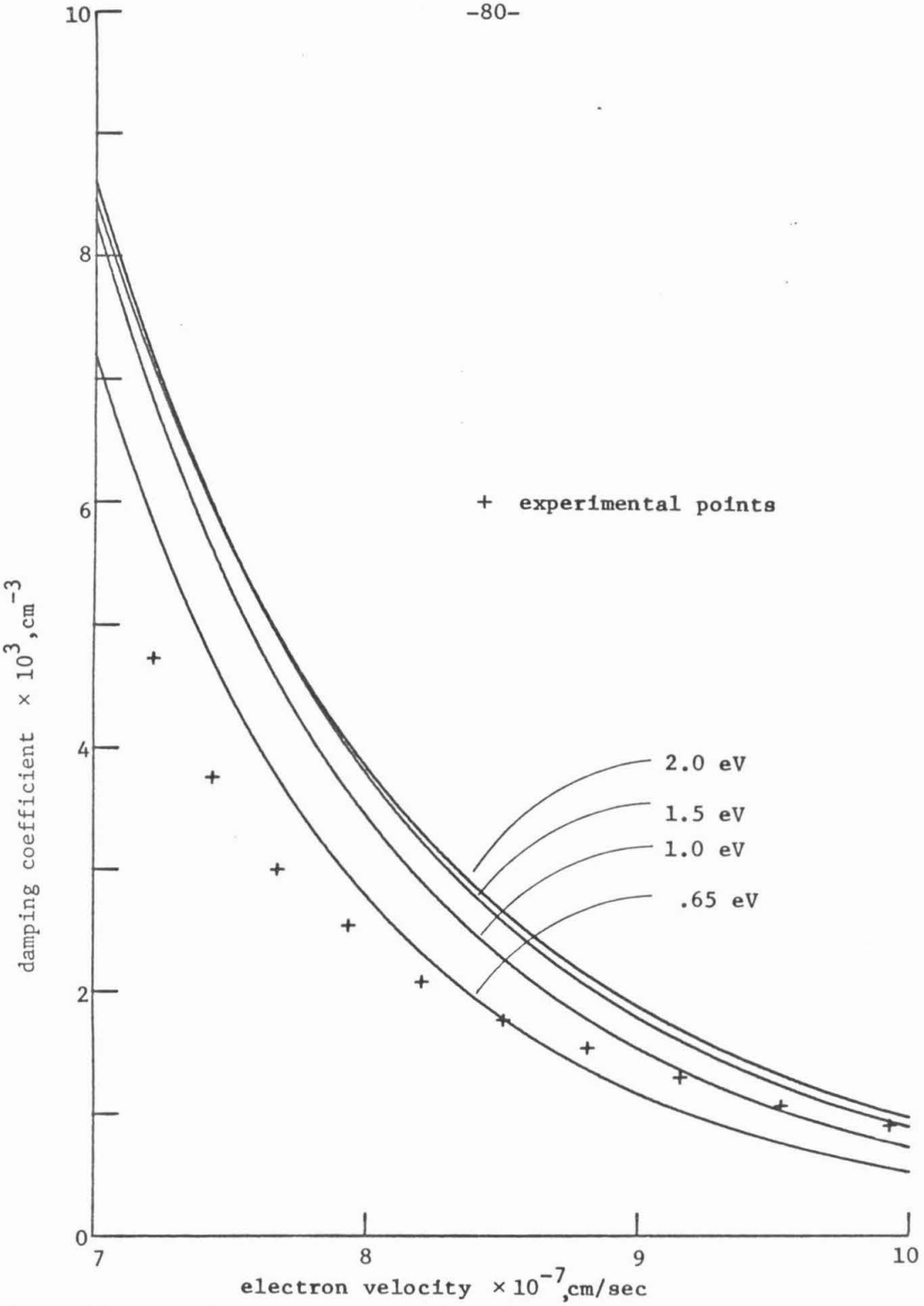

Fig. 14b. Damping exponent predicted from $D_{||}$ for an isotropic plasma.

As for the diffusion coefficient in a finite magnetic field, although the formal expression for it has been obtained by several people (Rostoker [35], Yelonskii [36]) it is difficult to evaluate except in certain limits (Rostoker [37]), none of which are appropriate here. The qualitative effect of a finite field or diffusion along the field is to mix what, in an isotropic plasma, are the parallel and perpendicular coefficients $D_{||}$ and $D_{\perp}$. D_{33} is analogous to $D_{||}$, which has a stronger velocity dependence than $D_{\perp}$. It is therefore possible that a correct finite field calculation would yield better agreement.

For purposes of comparison, a plot similar to Figure 14a using $D_{||}$ with the experimentally determined density is shown in Figure 14b.

CHAPTER 4. CONCLUSION

In this thesis several phenomena dealing with the spatial plasma wave echo have been experimentally studied as a function of the velocity of the electrons contributing to the echo by examining the spatial Fourier transform of the echo amplitude. It proved possible to get good agreement with theoretical predictions for those phenomena whose prediction did not require a knowledge of the equilibrium electron velocity distribution.

The echo amplitude saturation, which does not depend on the equilibrium distribution, showed the predicted Bessel function dependence on the second exciter potential. This agreement verified the contention of Sections 1.3 and 1.4 that a given spatial Fourier component of the echo corresponded to a particular electron velocity. The exciter electric field deduced from the saturation data was found to fit a simple $[\frac{\sin kh/2}{hk/2}]^2$ behavior. This implied that the plasma dielectric function was unimportant at the grids, as was expected theoretically.

Working at applied amplitudes for which saturation was negligible, the echo was studied as a function of exciter separation ℓ . For small exciter separation, echo damping due to diffusion in velocity space was also negligible, so that it was trivial with a knowledge of the equilibrium electron distribution to calculate the echo shape using the exciting fields given from the saturation measurement. The calculated shape of the undamped echo only agreed in detail with the observed echo for temperatures much higher than given by the ion-acoustic waves, suggesting the equilibrium distribution function was not Maxwellian.

The predicted $\exp[-b\ell^3]$ dependence of the damping on exciter separation ℓ was observed for each Fourier component of the echo, where b was a function of wave number, or equivalently, of velocity. However, the observed velocity dependence of b was somewhat weaker than that predicted for a Maxwellian electron distribution.

This discrepancy between theory and experiment can be accounted for in two possible ways. The most likely is that the high energy tail of the electron velocity distribution falls off more slowly with increasing energy than for a Maxwellian distribution, a conclusion which is also suggested from the echo shape. The other possibility is that the approximation of an infinite magnetic field in the calculation of the velocity space diffusion coefficient was poor and the effect of a finite magnetic field should be taken into account. It is difficult to determine the accuracy of this approximation because of the complexity of the calculations for a finite magnetic field.

Although the velocity dependence of the damping was not in good agreement with that predicted, that the observed damping was approximately equal in magnitude to that predicted indicates that the plasma was relatively free of turbulence.

To further assess the usefulness of this method of measuring the velocity dependence of diffusion in velocity space, it would be desirable to redo this experiment in a plasma of known equilibrium velocity distribution, or in a plasma where diffusion from externally produced turbulence (due to broad band noise, for example) dominated the diffusion from Coulomb collisions.

Appendix 1

This appendix gives the details of a one-dimensional calculation of the echo perturbed distribution for large amplitudes by the method of Coste and Peyraud [11], corresponding to Chapter I, Section 1.4.

Rather than using the Vlasov equation, this method considers the effect of the perturbed motion of the individual electrons on their equilibrium distribution function. Specifically, consider a perturbing region of finite extent in the plasma such that an electron traveling towards this region with velocity v_o leaves it with velocity $v = v_o + \Delta v(x,v,t)$. Provided $|\Delta v| < v_o$, if the unperturbed distribution function for electrons traveling towards this region is $f_o(v)$, the distribution function of the electrons leaving the region will be $f_o(v - \Delta v(x,v,t))$. This method uses a perturbation series in $\Delta v/v$, a quantity which is easily made small experimentally.

Because the perturbed distribution depends on x, v, and t , while the initial distribution only depends on v_o , it is convenient to work backwards, starting with a given (x,v,t) and finding the corresponding v_o .

Consider the unperturbed electrons to be coming from the left. The equation of motion of the electron is $\dot{v}(t) = \frac{e}{m} E(x(t),t)$, where e and m are the charge and mass of the electron. It is more convenient to have the position the free parameter, in which case

$\frac{dv}{dx} = \frac{e}{m}\frac{E(x,t(x))}{v(x)}$. If the region in which $E \neq 0$ is small, one can approximate $t(x)$ by the free motion in the argument of E, in which case $t = t_2 + (x-x_2)/v_2$; (x_1,v_1,t_1) and (x_2,v_2,t_2) refer to the left hand and right hand values of position, velocity, and time (where $E = 0$).

Integrating, one has $v_2 - v_1 = \frac{e}{mv_2}\int_{x_1}^{x_2} E(x,t_2 + (x-x_2)/v_2)dx_2$. Assuming the excitation E is at a fixed frequency ω_2 , $E(x,t) = \mathrm{Re}[E_{\omega_2}(x)\exp(-i\omega_2 t)]$, where Re means the real part. Then

$$v_2 - v_1 = \frac{e}{mv_2}\mathrm{Re}\{\exp(-i\omega_2(t_2 - (x_2-\ell)/v_2))\int_{x_1}^{x_2} E_{\omega_2}(x) \times \exp(-i\omega_2(x-\ell)/v_2)dx\} \qquad (1)$$

where $E(x,t)$ is localized about $x = \ell$.

The limits of the integral in (1) can be extended to $\pm\infty$ without changing its value, which makes it the Fourier transform of $E_\omega(x)$, so that

$$v_2 - v_1 = \frac{e}{mv_2}\mathrm{Re}\{\exp(-i\omega_2(t_2 - (x_2-\ell)/v_2))\,\tilde{E}(\omega_2/v_2,\omega_2)\} \quad . \qquad (2)$$

$E_\omega(x)$ will be a combination of the applied and self-consistent fields, but for (2) to be valid, its width Δx must be such that $\frac{\Delta x}{v_2}\frac{\Delta v}{v_2} << \frac{2\pi}{\omega_2}$. That is, the error in using the free motion should not produce a large phase shift.

Another exciter at $x = 0$ at frequency ω_1 will similarly produce a change in velocity

$$v_1 - v_o = \frac{e}{mv_1} \text{Re} \{\exp(-i\omega_1(t_1 - x_1/v_1))\ \tilde{E}(\omega_1/v_1, \omega_1)\} \qquad (3)$$

Assuming the time required to travel from x_1 to x_2 is $t_2 - t_1 = (x_2 - \ell)/v_2 + (\ell - x_1)/v_1$, (3) can be expressed as

$$v_1 - v_o = \frac{e}{mv_1} \text{Re} \{\exp(-i\omega_1(t_2 - \ell/v_1 - (x_2 - \ell)/v_2))\ \tilde{E}(\omega_1, \omega_1/v_1)\} \qquad (4)$$

For future convenience the electric fields will be expressed as

$$E(\omega_1/v_1, \omega) = \mathcal{E}_1 \exp[i\theta_1] \quad \text{and} \quad E(\omega_2/v_2, \omega_2) = \mathcal{E}_2 \exp[i\theta_2]$$

where $\mathcal{E}_1$ and $\mathcal{E}_2$ are real and positive. Letting $v_2 - v_1 = \Delta v_2$, $\ell/v_1 \cong \ell/v_2(1 + \frac{\Delta v_2}{v_2})$.

Combining (2) and (4), one then has

$$v_2 - v_o \equiv \Delta v = \Delta v_2 + \frac{e}{mv_1}\mathcal{E}_1 \text{Re} \{\exp[-i\omega_1(t_2 - x_2/v_2) + i\theta_1] \times \exp[i\omega_1 \ell \Delta v_2/v_2^2]\} \qquad (5)$$

The echo results from the latter exponential in (5), which can be evaluated using the generating function for the Bessel function,

$$\exp[iz \sin\theta] = \sum_{n=-\infty}^{\infty} J_n(z) \exp[in\theta] .$$

Using (2), one then has

$$\exp[i\omega_1 \ell \Delta v_2/v_2^2] = \sum_{n=-\infty}^{\infty} J_n\left(\frac{\omega_1 \ell e}{v_2^3 m}\right) \exp[in(\tfrac{\pi}{2} + \theta_2 - \omega_2(t_2 - (x_2 - \ell)/v_2))] \qquad (6)$$

Substituting (6) into (5) gives

$$\Delta v = \Delta v_2 + \frac{e}{mv_1} \mathcal{E}_1 \sum_{n=-\infty}^{\infty} J_n\left(\frac{\omega_1 \ell e \mathcal{E}_2}{v_2^3 m}\right)$$

$$\text{Re } \exp[in\pi/2 + i(n\theta_2+\theta_1) - i(\omega_1 + n\omega_2)t_2$$

$$+ i(n\omega_2(x_2-\ell) + \omega_1 x_2)/v_2] \qquad (7)$$

Assuming $\Delta v << v$, $f_o(v-\Delta v) \tilde{=} f_o(v) - \frac{\partial f_o(v)}{\partial v} \Delta v$. The term in (7) corresponding to the second order echo is that with frequency $\omega_2 - \omega_1 = \omega_3$, which is

$$\Delta v(x_2, v_2, \omega_3) = \frac{e}{mv_1} \mathcal{E}_1 J_1\left(\frac{\omega_1 \ell e \mathcal{E}_2}{v_2^3 m}\right)$$

$$\times \quad \text{Re } i \exp[i(\theta_2-\theta_1) + i(\omega_2(x_2-\ell) - \omega_1 x_2)/v_2] \qquad (8)$$

To first order in this perturbation expansion, the v_1's in Δv can be replaced by v_2's . θ_1 and θ_2 will in general vary with v_2 , with the dependence determined by the dielectric function.

LIST OF REFERENCES

1. L. D. Landau, J. Phys. USSR 10, 25 (1946)
2. N. G. vanKampen and B. U. Felderhof, Theoretical Methods in Plasma Physics (Wiley, New York, 1967)
3. R. W. Gould, Phys. Rev. 136, A991 (1964)
4. A. Y. Wong et al., Phys. Rev. 133, A436 (1964)
5. J. H. Malmberg and C. B. Wharton, Phys. Rev. Letters 6, 184 (1964)
6. J. H. Malmberg et al., in Plasma Physics and Controlled Nuclear Fusion Research (I.A.E.A., Vienna, 1966), Vol. I, p. 485
7. R. W. Gould et al., Phys. Rev. Letters 19, 219 (1967)
8. R. W. Gould, Phys. Letters 25A, 559 (1967)
9. T. M. O'Neil and R. W. Gould, Phys. Fluids 11, 134 (1968)
10. A. Y. Wong et al., Phys. Rev. 133, A436 (1964)
11. J. Coste and J. Peyraud, J. Plasma Phys. 3, 603 (1969)
12. J. H. Malmberg et al., Phys. Rev. Letters 20, 95 (1968)
13. H. Ikezi et al., Phys. Fluids 12, 853 (1969); and H. Ikezi and N. Takahashi, Phys. Rev. Letters 20, 140 (1968)
14. D. R. Baker et al., Phys. Rev. Letters 20, 318 (1968)
15. V. I. Karpman, Soviet Phys. JETP 24, 603 (1967)
16. C. H. Su and C. Oberman, Phys. Rev. Letters 20, 427 (1968)
17. T. Dupree, Phys. Fluids 9, 1773 (1966)
18. T. M. O'Neil, Phys. Fluids 11, 2420 (1968)
19. K. Nishikawa and R. W. Gould, Phys. Fluids 13, 1883 (1970)
20. F. L. Hinton and T. Kawabe, Phys. Fluids 13, 1212 (1970)
21. A. Y. Wong and D. R. Baker, Phys. Rev. 188, 326 (1969)
22. M. Guillemot et al., Phys. Fluids 14, 2065 (1971)
23. T. H. Jensen et al., Phys. Fluids 12, 1728 (1969)

24. A. G. Sitenko, Electromagnetic Fluctuations in Plasma (Academic Press, New York, 1967)

25. L. Spitzer, Physics of Fully Ionized Gases (Interscience Publishers, Inc., New York, 1956)

26. R. B. Brode, Rev. Mod. Phys. 5, 257 (1933)

27. D. A. Dunn, et al., JAP 36, 3273 (1965)

28. A. Hirose et al., ORNL-4401, p. 136 (1968)

29. S. A. Self, JAP 40, 5217 (1969)

30. R. S. Harp, Rev. Sci. Instr. 34, 416 (1963)

31. B. D. Fried and S. D. Conte, Plasma Dispersion Function (Academic Press, New York, 1961)

32. R. K. Fisher and R. W. Gould, Phys. Fluids 14, 857 (1971)

33. C. M. Rader and B. Gold, Proc. IEEE 55, 149 (1967)

34. J. W. Cooley and J. W. Tukey, Math. of Comp. 19, 297 (1965)

35. N. Rostoker and M. Rosenbluth, Phys. Fluids 3, 1 (1960)

36. V. M. Yelonskii et al., Soviet Phys. JETP 15, 619 (1962)

37. N. Rostoker and M. Rosenbluth, General Atomic Report GAMD-663, part III.